A shale-hosted Cr isotope record of low atmospheric oxy-gen during the Proterozoic

Devon B. Cole et al.

Supplementary Information

SI 1.

Methods

Sample Preparation:

All samples were either from drill core or from the least altered portions of outcrop samples, selected for lowest possible degree of weathering. Handsamples were then cut with a diamond edge rock saw, with surfaces coming in contact with saw blade sanded away after cutting. Cut samples were crushed in an agate mill to a fine powder. For total digests, sample powders were ashed at 500°C for 8 hours to remove organic matter. Ashed samples were then digested at 90°C using a concentrated HF-HNO_3 mixture followed by aqua regia digestion of dried residues. Final residues were dissolved in 5 ml 6N HCl for stock solutions. For leaches, sediments were subjected to a cold 3N HNO_3 leach for ~24 hours as developed by (Reinhard et al., 2014).

Elemental Concentrations:

Major and trace elements for total digests and nitric acid leaches were analyzed in the Department of Geology and Geophysics at Yale University by ICP-MS (Element XR, Thermo-Finnigan) using a standard sample introduction system. An aliquot of the 6N HCl stock solutions obtained after total digests (see below) was diluted in 5% HNO_3, and Cr and Ti were measured in medium resolution. Measurement precision was generally better than 4% for major and trace elements and USGS geostandards BHVO-2 and NOD-A-1 processed along with samples during each run are within 10% of reported values.

Chromium Isotope Analyses:

The method for chromium isotope analysis is based on that of (Schoenberg et al., 2008). Chromium isotope compositions were determined for both bulk sediment and leach fractions of samples from the Doldgeville Formation, Tal formation, Black River Dolomite (Tongari Group), Doushantou Formation, Walcott and Awatubi Formations (Chuar Group), Simla Formation, Arctic Bay Formation, Xiamaling Formation, Velkerri Formation, Barney Creek Formation, Mount Les Siltstone Formation, Lady Lorretta Formation, Damtha Group, Timeball Hill Formation, Roy Hill Shale member (Jeerinah Formation), Mount McRae Shale, and Mount Sylvia Formation. Chromium isotopes were measured by MC-ICP-MS using a double-spike correction for instrumental mass bias. A mixture of ^{50}Cr and ^{54}Cr isotopes was added to the samples prior to Cr separation on chromatographic columns, with a constant spike/sample ratio of ~0.5. The following protocol includes three separation steps (Reinhard et al., 2014; Schoenberg et al., 2008) that ensure complete removal of Fe, Ti and V during chemical separation in order to avoid major isobaric interferences of ^{54}Fe, ^{50}Ti and ^{50}V on Cr isotopes during analysis.

In the first step, a split of the 6N HCl stock solution was spiked and evaporated until dry. Residues were brought up in 1N HCl. Since only Cr(VI) is retained on the column, complete oxidation of Cr(III) to Cr(VI) was ensured through addition of potassium peroxidisulfate and allowing the reaction to proceed for 2 hours at 110°C. Any iron precipitates were removed by centrifuging. Columns were loaded with 2 ml AG1-X8 anionic resin (100-200 mesh), which was then cleaned with mQ water, 3N HNO_3 and 6N HCl. The matrix was then eluted with 24 ml of 0.2N HCl and 4 ml 2N HCl, with Cr

subsequently collected with 5 ml 2N HNO_3 and 0.5% H_2O_2.

The second step removes any trace Fe that may remain after the first elution. Microcolumns filled with 0.2 ml AG1-X8 resin were cleaned with mQ water and 3N HNO_3, and samples were loaded and collected with 1.2 ml 6N HCl.

In the final step, trace Ti was removed using a cationic resin AG50W-X8 (200-400 mesh). The resin was cleaned with mQ water, 3N HNO_3 and 6N HCl followed by matrix elution with 1 ml 0.5N HNO_3, 2 ml 0.5N HF and 6 ml 1N HCl, and Cr was finally collected with 5 ml 1.8N HCl. Residues were redissolved in 5% HNO_3 for MC-ICP-MS analysis.

Chromium isotopes were measured on a Neptune Plus (Thermo-Finnigan) MC-ICP-MS at Yale University according to the analytical protocol of (Schoenberg et al., 2008). Samples were run in high-resolution mode to resolve polyatomic interferences such as $^{40}Ar^{12}C^+$, $^{40}Ar^{14}N^+$ and $^{40}Ar^{16}O^+$. Although our chemical procedure should ensure complete removal of Fe, Ti and V, the presence of these three elements was monitored by measuring ^{56}Fe, ^{49}Ti and ^{51}V, which were used to correct our samples for potential interferences of ^{54}Fe on ^{54}Cr, and ^{50}Ti and ^{50}V on ^{50}Cr. Standard-sample-bracketing was employed during each analytical session by measuring a spiked Cr isotope standard NIST SRM 979 before and after each natural sample. Chromium levels in blanks run with each batch were negligible compared to that of samples. Chromium isotope ratios are reported relative to bracketing standards using conventional delta notation ($\delta^{53/52}Cr = [(^{53}Cr/^{52}Cr)_{sample}/(^{53}Cr/^{52}Cr)_{NIST\text{-}979} - 1] \times 1000‰$). Addition of double-spike to the samples allows for correction of potential Cr isotope fractionation during chromatographic separation, as well as correcting for instrumental mass bias that occurs during introduction of the sample to the mass spectrometer. The double-spike data reduction model is based on the iterative method described by (Siebert et al., 2001).

External precision is reported as two sigma (2σ) uncertainty, and is calculated based on duplicate analyses of geological reference materials (GRM) processed through ion-exchange chromatography columns along with samples (BHVO-2 and Nod-A-1 were systematically processed with 18 samples). The measured $\delta^{53}Cr$ value for BHVO-2 is -0.12 ±0.06‰ and Nod-A-1 has a $\delta^{53}Cr$ value of 0.07 ± 0.08‰ which are similar to published values in the literature (Schoenberg et al., 2008). Sample duplicates including column procedure duplicates, digested duplicates, and replicate measurements on the MC-ICP-MS allow a calculation of a 2RMS (root mean square) of 0.06‰ on the delta values. In addition, a two-standard deviation of the mean (2se) is systematically calculated using the 50 cycles of measurement obtained for each sample during MC-ICP-MS analysis and is generally on the order of 0.02 ‰ on the delta values.

SI 2.

Previous work on mid-Proterozoic atmospheric oxygen levels

Earlier attempts to quantitatively estimate atmospheric oxygen levels through the mid-Proterozoic are discussed in the main text (e.g. (Holland, 2006; Rye and Holland, 1998; Sheldon, 2013)), along with previous attempts to reconstruct pO_2 using the Cr isotope system ((Crowe et al., 2013; Frei et al., 2009; Planavsky et al., 2014). However, we would like to expand our discussion of most recent work by Zhang et al. (2016a), which proposes atmospheric oxygen levels of ~4% PAL at 1.4 Ga, and revisit the suggestion of Zhang et al. (2016b) of fundamental flaws with previous Cr isotope work.

There are a number of potential problems with the findings of Zhang et al. (2016), as discussed by Planavsky et al. (2016). Firstly, Zhang et al. (2016) infer oxic deposition based on small depletions in V/Al ratios relative to the modern crustal average. However, such variation can easily be accounted for by variation in detrital flux (as demonstrated in modern topsoils (Planavsky et al., 2016)). In addition, Zhang et al. (2016, 2016b) make no attempt to justify the assumption that the V/Al ratio of the detrital flux was constant over the ~400,000 years of deposition represented by their geochemical record. Secondly, the biomarker data of Zhang et al. (2016) does not meet currently accepted standards for Precambrian biomarker work (e.g. (French et al., 2015), and conflicts with both previous work on the same formation (Luo et al. 2015), as well as recent biomarker records from other mid-Proterozoic rocks (1.7-1.0 Ga) from China, Australia, and Mauritania, which indicate no detectable steranes/methylsteranes despite detection of abundant bacterially derived hopanes (e.g. (Flannery and George, 2014; Luo et al., 2015). Given this contrast, the burden of proof for syngeneity of biomarker signals with the host rock is elevated for Zhang et al. (2016). Both compound classes (2,3,6-TMAIs and steranes) are known to be common contaminants in Precambrian sedimentary rocks (Illing et al., 2014) and demand extreme care in their use as paleoenvironmental proxies, which typically includes parallel analysis of the bound biomarker pool from kerogen (Love et al., 2009). Because Zhang et al. (2016) do not include kerogen analysis or follow the lead of recent organic geochemical research on Precambrian strata (e.g., French et al., 2015), their data should be viewed with caution (Planavsky et al., 2016).

Additionally, brief intervals of high oxygen are unlikely to create an evolutionary landscape favorable for animal evolution, as suggested by Zhang et al. (2016). Although we are suggesting a baseline of low, animal-precluding oxygen levels for much of the mid-Proterozoic, it is important to note that none of the existing data preclude transient intervals of higher oxygen (Planavsky et al., 2014). In fact, as noted in the main text, some small Proterozoic Cr isotope variations may be linked to Cr redox cycling. Further, a smaller atmospheric oxygen reservoir as we envision for the mid-Proterozoic would exhibit less capacity to resist change compared to the Phanerozoic and therefore may have been characterized by dynamic variance around still low baseline pO_2 levels. Although the work of Zhang et al. (2016) is inconclusive in this regard, we nevertheless expect to find evidence of such episodes. However, it is the periodicity and persistence of low environmental oxygen levels that are likely to be the key factor in governing the evolutionary landscape during the early emergence and ecological expansion of animals, not merely the existence of brief intervals of high oxygen (Reinhard et al., in press).

Lastly, Zhang et al. (2016b) suggest that a linear relationship between Cr and Ti enrichments in marine sediments is evidence of a purely detrital signature with no authigenic component. The authors attempt to demonstrate this with Cr and Ti concentration data from laser ablation of the samples used in the study of Planavksy et al. (2014), qualifying (also linear) enrichments above the slope of the crustal average Cr/Ti – in three out of the four formations considered – as evidence of detrital variability. To better understand this pattern, we have compared Cr and Ti concentrations of the iron-rich chemical sediments of Planavsky et al. (2014), all samples of our shale record, and samples from the Demerara Rise (Planavsky et al., 2014) – considered a type case for authigenic enrichment (Fig.1). There is an extremely large range for potential Cr/Ti ratios in marine sediment, extending even below the crustal average ratio (which we would

expect, see below). Secondly, a linear relationship between Cr and Ti is observed in the highly enriched Demerara Rise sediments, which we would also expect, considering this ratio is derived from the mixing of a (relatively) consistent detrital signature and a (relatively) consistent authigenic enrichment. The slope of the relationship between Cr and Ti will be controlled by sedimentation rate and potential for Cr scavenging, with deviation from that slope indicating variation in either of these controlling factors.

Figure 1:

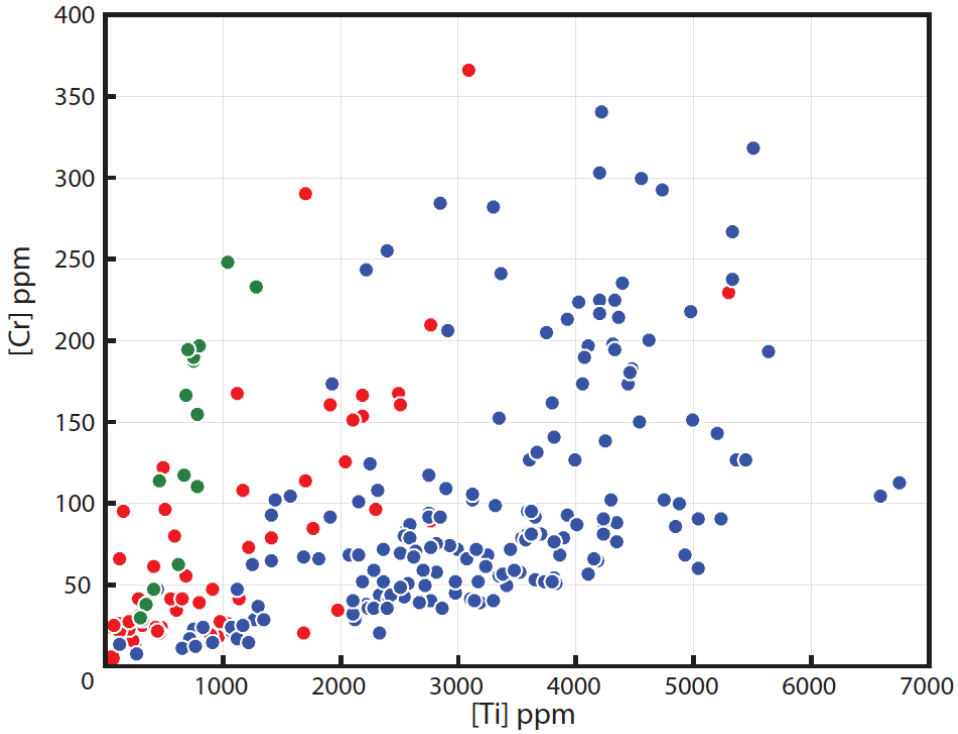

Figure 1: Cr enrichments in shales and iron-rich chemical sediments. Concentrations of Cr versus Ti for all shale samples of this study (blue), all iron-rich chemical sediments of Planavsky et al. (2014) (red) and Demerara Rise samples of Planavsky et al. (2014) (green).

SI 3.

Potential for detrital influence on δ^{53}Cr measurements

Many redox sensitive metals, including Cr, have both a detrital and authigenic component in marine sediments. Broadly, enrichments in the authigenic fraction are influenced by redox conditions in the marine system, while the detrital contribution is considered to be unaffected and relatively constant. Thus, in the Cr system, it is the authigenic fraction that has the potential to preserve fractionations produced during terrestrial oxidative weathering, signaling increased pO_2, while the detrital fraction should negligible isotopic fractionation from the bulk silicate earth value of $\delta^{53}Cr = -0.124 \pm 0.101‰$ (Schoenberg et al., 2008; Gueguen et al., 2016). Traditionally, the continental crust average Cr/Ti value of ~0.02 (Rudnick and Gao, 2014) is used as a cutoff value to characterize the detrital contribution to marine sediments and values above ~0.02 are considered evidence

of authigenic enrichment. Unfortunately, the use of this single average value fails to consider the significant variability over large geographic areas possible in the detrital flux of Cr to the ocean, and excludes the potential for recognizing small but measurable authigenic enrichments that would be expected through much of the mid-Proterozoic. An excellent example of this is apparent in the Peru Margin sediments (Gueguen et al., 2016), where despite low Cr/Ti ratios (values that would be considered depleted compared to the crustal average), significant authigenic enrichments are clearly observed. Oxic marine sediments also display a large range of Cr/Ti ratios and often values below the crustal average (Gueguen et al., 2016). Thus, it is apparent that such depletions in the detrital contribution to marine sediments can easily conceal the relatively muted authigenic enrichments we would expect in mid-Proterozoic shales (i.e Reinhard et al., 2013). Considering the lack of utility for using a single crustal cutoff value to fingerprint authigenic enrichment in this context, we have instead employed a statistical comparison of pre- and post- 800 Ma samples within a single Cr/Ti range to test the validity of our δ^{53}Cr results (see below).

SI 4.

Statistical Analysis

To determine if there is a statistically significant difference in the δ^{53}Cr values and binned Cr/Ti ratios in pre and post 800 Ma black shales we have performed *t*-tests and bootstrapped resampling of mean values (n=10,000). We have compared two bins: samples from 0 to 800 Ma (stage 1) to samples from 800 to 1800 Ma (stage 2) within a defined bulk rock range of Cr/Ti [0.015-0.025]. Within the chosen bin, both stages retain a roughly normal distribution. The bootstrap resampled means of the stage 1 Cr/Ti ratios compared to the Cr/Ti of stage 2 samples within this range overlap significantly in their 95% confidence intervals (Fig. 2a, main text). As there is no evidence for a shift in the Cr/Ti ratio of the upper continental crust from the Proterozoic to the Cenozoic (see main text), and thus with sufficient sampling there should be an equal chance of capturing fractionated δ^{53}Cr values in either time bin. Despite this potential, the resampled means of δ^{53}Cr values for both stages show no overlap in their 95% confidence intervals, and the resampled means for the Mesoproterozoic fall entirely within the unfractionated range of bulk silicate earth (Fig. 2b, main text). A two-tailed *t*-test was also performed which failed to reject the null hypothesis that both time bins have equal means (p = 0.15). These results emphasize the validity of our observed baseline shift as a real authigenic signal, and support the robust nature of our data set.

Additionally, we have demonstrated that over the wide range of Cr/Ti values through our pre-1.0 Ga samples, there is no relationship with δ^{53}Cr, producing a p-value of 3.2×10^{-49}. We have illustrated the continuity of the data in Figure 2.

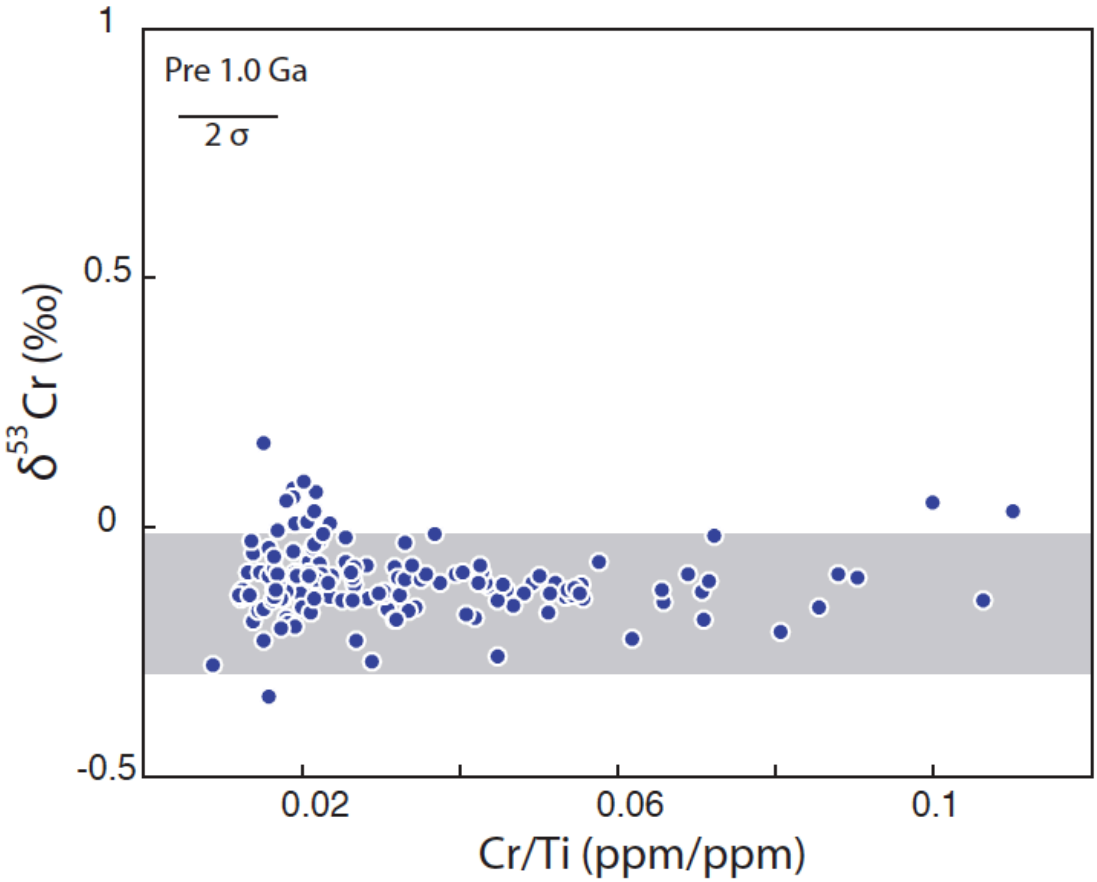

Figure 2. No relationship between Cr/Ti and δ^{53}Cr. All pre - 1.0 Ga data of this study. Bulk silicate Earth δ^{53}Cr values represented by the grey bar.

SI 5.
Sample Localities and Descriptions

The 0.45 Utica Shale, New York, USA

The middle Ordovician Utica Shale of New York state is divided into three members – the Flat Creek member, the Doldgeville member, and the Indian Creek member. The middle Doldgeville member was sampled for this study at the Doldgeville dam in Doldgeville, NY. Based on careful graptolite biostratigraphic correlations, the Doldgeville member has been assigned to the lower upper Ordovican *O. ruedemanni* zone in the Mohawkian (Goldman et al., 1994; Lehmann et al., 1995; Ruedemann, 1908).

The 0.55 Tal Group, Northern India

The Tal Group is exposed in a number of northwest striking synclines in the Krol belt of the Lesser Himalaya region of northwestern India. Based on detailed biostratigraphy precise constraints have been placed on the age, placing the lower black shale member (from which our samples were taken) in the earliest Cambrian Meishucunian stage (Hughes et al., 2005). Additionally, two coherent Re-Os isochrons for the underlying Krol-Tal (Precambrian-Cambrian) boundary have been reported – 554 ± 16 Ma and 552

± 22 Ma – indicating minimal mobilization of metals during any post depositional alteration (Singh et al., 1999). The samples of the lower black shale member of the Tal used in this study were collected on the east bank of the Ganges in the town of Kaudiyala on the Haridwar Rishikesh Badrinath road at N 30.040559°, E 78.300400°. The section was freshly exposed due to recent flooding, providing unweathered surfaces.

The 0.63 Ga Doushantou Formation, South China

The Ediacaran Doushantou Formation of South China is described in the Yangtze Gorges area, and has been broken into four members (Chuanming et al., 2007; McFadden et al., 2008; Zhu et al., 2007). Member I is identified as the cap carbonate of the basal Doushantou. The samples of this study are from Member II, which consists of alternating organic-rich shale and carbonate. This unit is overlain by Member III which designates a shift to predominantly carbonate deposition, and finally Member IV, a 10m thick organic rich shale which caps the formation (Sahoo et al., 2012). Our samples were used in previous studies (Sahoo et al., 2016; Sahoo et al., 2012) and are from the Wuhe section, Guizhou province, with an estimated depositional age between 635 – 630 Ma, with a maximum age of 635.2 ± 0.6 Ma (Condon et al., 2005) from an ash bed within Member I and a minimum age of 614 ± 7.6 Ma (Liu et al., 2009) from the middle Doushantou Formation [see (Sahoo et al., 2012), supplementary information, for further discussion]. Despite the anoxic depositional environment based on iron speciation data (Sahoo et al., 2012), the lack of authigenic redox sensitive metal enrichments (including Cr/Ti ratios well below upper continental crust values of 0.2) may explain the lack of a fractionated signal our δ^{53}Cr data.

The ~0.64-0.8 Ga Black River Dolomite, NW Tasmania

The Julius River Member of the Black River Dolomite is part of the Tongari group of northwestern Tasmania. The Julius River is composed of two diamictite horizons separated by a mixed limestone and shale interval, and overlain by an undifferentiated pyritic shale (Calver, 2011). The Black River Dolomite has been correlated with the Sturtian glaciation (Calver, 1998; Kendall et al., 2009a), and our samples from the Forest-1 drill core in the Smithton Synclinorium as described by (Abbott and Sweet, 2000; Calver, 1998; Kendall et al., 2009a; Riedman et al., 2014), range from pre-glacial to post-glacial. The uppermost Julius River has produced a Re-Os age of 640.7 ± 4.7 Ma (Kendall et al., 2009a), giving a minimum depositional age for the Julius River Member, considering no unconformity between the members. The Re-Os isochron of (Kendall et al., 2009a) is indicative of well preserved strata and a lack of mobility of trace metals in later-stage fluids. Our samples from within the Julius River Member are likely to have an age ca.700 Ma if the correlation with the Sturtian is correct, based on Sturtian ages 716.5 ± 0.24 Ma, 716.4 ± 0.54 Ma, and 717.4 ± 0.14 Ma (Macdonald et al., 2010). If the correlation between the base of the Julius River and the top of the Bitter Springs formation is correct (Riedman et al., 2014), we can use the upper Bitter Springs date of 811.51 ± 0.25 Ma to constrain our pre-glacial samples to ~ 811 Ma.

The 0.74 Ga Chuar Group, Arizona, USA

The Chuar Group, exposed only in the Grand Canyon, USA represents deposition in an intracratonic rift basin during extension in the middle Neoproterozoic (Dehler et al.,

2001; Karlstrom et al., 2000). An ash layer from the uppermost Chuar has yielded a zircon age of 742 ± 6 Ma (Karlstrom et al., 2000). Our samples come from the Walcott Member, which is capped by the dated ashbed, and the underlying Awatubi Member. These members of the Kwagunt Formation are composed of organic rich shales, which have famously yielded vase-shaped microfossils (VSMs), and thus the earliest fossil evidence for marine heterotrophic eukaryotes and eukaryotic diversification (Karlstrom et al., 2000; Porter and Knoll, 2000). The preservation of such fossils, as well as coherent paleomagnetic data including a positive fold test on the Chuar syncline (Karlstrom et al., 2000) are indicative of well-preserved and very low grade strata well suited for trace metal analyses.

The ~ 0.84 Simla Group, Northern India

The Simla Group is exposed in the outer lesser Himalaya of Northern India and has provided a Re-Os age of 839 ± 139 (Singh et al., 1999). The Simla is comprised primarily of siltstones and shales with some more organic-rich intervals. Interbedded sandstones are also present. Our samples were collected at four localities; the first in the Yamuna River valley at N 30.534306°, E 77.906611°, the second on the Simla – Kanga road just north of Bagha at N 31.188918°, E 76.988983°, the third in the Tons river valley just north of Killor at N 30°561624, E 77°.817923, and the fourth on the road between Theog and Matiana beginning at the trash dump at N 31.070550°, E 77.223405°.

The ~ 1.1 Ga Arctic Bay Formation, Bylot Supergroup, Baffin Island

The Arctic Bay formation comprises fine-grained siliclastic sediment deposited on a tectonically active, northwest-deepening ramp as part of the Bylot Supergroup in the intracratonic Borden Basin. The Bylot Supergroup unconformably overlies Paleoproterozoic and Archean crystalline rocks of the Rae Province and is crosscut by Franklin-age dikes (~ 723 Ma) (Denyszyn et al., 2009; Jackson and Iannelli, 1981). The Bylot Supergroup is exposed on northern Baffin and Bylot islands. The Arctic Bay formation ranges in thicknesses from >1000m in the southeast to ~300m in the northwest due to lateral facies variation, and has yielded a whole rock U-Th-Pb age of ~1.1 Ga (Turner and Kamber, 2012). In all locations, meter-scale shallowing-upward cycles are preserved through the lower part of the formation before grading upward into predominantly shale as a result of an overall deepening of the basin. The Arctic Bay formation conformably overlies Adams Sound formation sandstone and basal Nauyat formation basalt, which is presumed to be equivalent to the ~1.27 Ga Mackenzie dike swarm (LeCheminant and Heaman, 1989).

In the deeper, northwestern portion of the basin, the Ikpiarjuk formation represents localized, time equivalent carbonate mounds within Arctic Bay formation shale and deep-water carbonates of the Nanisivik formation directly overlie the Arctic Bay and Ikpiarjuk formations. In the shallower portions of the basin to the southeast, the Iqqittuq formation carbonate ramp progrades over the Arctic Bay formation before the development of a rimmed carbonate platform, represented by the Angmaat formation. Samples for this study come from 2 correlative stratigraphic sections taken though the Arctic Bay formation along the length of the Milne Inlet graben. Sections PWC1405 and MB1401(N72°23’43.8’’, W081°11’22.1”) form a composite section in the central Miln Inlet graben and T1413 (N 72° 45’ 04.8’’ W 083° 50’39.2”) is from the deepest

portion of the basin in northwestern Milne Inlet graben. Sampling through these sections targeted the freshest material and the finest, most organic rich beds. We have performed a detailed analysis of Cr isotopes through both of these thick stratigraphic sections and have demonstrated the stratigraphic continuity of the observed Cr signal in both bulk and leach analyses (Fig. 3).

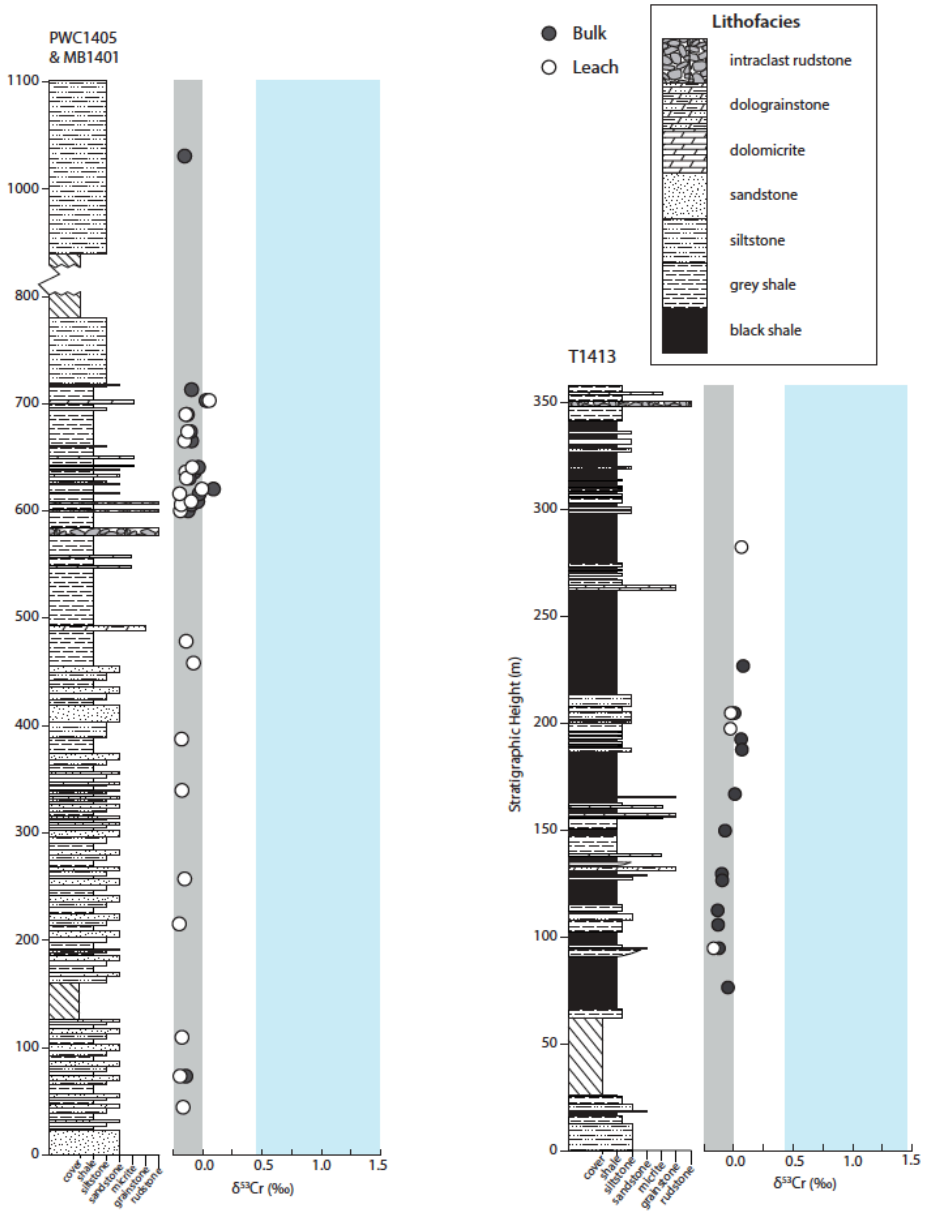

Figure 3. Arctic Bay Formation stratigraphic sections and Cr isotope data. Two measured sections of the Arctic Bay formation with Cr isotope data for both bulk (dark grey) and leach (white) analyses plotted in stratigraphic context. The range for bulk silicate Earth $\delta^{53}Cr$ values is represented by the grey bar (Schoenberg et al., 2008), while the blue bar shows the range for modern seawater (Scheiderich et al., 2015).

The 1.38 Ga Xiamaling Formation, North China

The Xiamaling formation sits unconformably between the Tieling and Changlongshan formations deposited on the North China craton. The Xiamaling formation is composed of four members, and our samples are from the third member. These samples are from the Xiaqian 1 (XQ1) core, which includes Members II-III, and is located just west of Zhuolu in the Western Hills of Beijing. Members II-III are ~ 105m in thickness and are comprised of organic-rich black shales and interbedded silty shales. The Xiamaling also contains a number of weathered ash beds, including two such beds through the third member yielding U-Pb zircon ages of 1379 ± 12 Ma and 1380 ± 36 Ma (Su et al., 2008).

The 1.4 Ga Velkerri Formation, Roper Group, Northern Australia

The Velkerri Formation is part of the Roper Group of Northern Territory, Australia deposited as part of the McArthur Basin. Our samples come from the Urapunga-4 core, and were previously used to obtain two Re–Os ages for the upper and lower parts of the formation (Kendall et al., 2009b). The lower interval, from 325.7 – 326.7 m, produced an age of 1417 ± 29 Ma, while the upper interval, from 136.9-137.9 m, produced an age of 1361 ± 21 Ma. The Velkerri formation has been interpreted as a deep marine facies deposited in an epicrationic basin well connected with the open ocean system (Abbott and Sweet, 2000; Jackson and Raiswell, 1991; Johnston et al., 2008). The coherent Re-Os isochrons of (Kendall et al., 2009b) indicate little to no post-depositional alteration or mobility of trace metals via hydrothermal fluids.

The 1.65 Ga Barney Creek, Mount Les Siltstone, and Lady Lorreta Formations, Northern Australia

The Barney Creek and Mount Les Siltstone formations were deposited as part of the ~1650 – 1570 Ma McArthur basin of the Northern Territory, Australia. The Lady Lorreta Formation was deposited as part of the coeval Mount Isa basin of Queensland Australia. Our samples consist of powdered 10 – 25cm lengths of three separate drill cores, consisting of laminated shales with infrequent silt interbeds. The Barney Creek samples are from the Myrtle prospect drill hole MY4, which has three tuffs dated at 1638 ± 7, 1639 ± 3, and 1640 ± 3 Ma (Page et al., 2000). The Mount Les samples dated at 1640 ± 7 Ma (Page et al., 2000) are from the WFDD84 core near the Walford Creek prospect. The Lady Lorreta formation samples are from the LA64 core of the Mt. Isa basin, and yield zircons dated at 1647 ± 4 Ma(Page et al., 2000). These samples have already been studied in detail and analyzed for iron speciation by (Planavsky et al., 2011), who have determined the selected samples to be unaltered by mineralizing fluids. See supplementary information of (Planavsky et al., 2011) for further discussion.

The ~1.7 Damtha Group, Northern India

The Damtha Group is exposed in the inner Lesser Himalaya and overlies the Berinag Group which has an interbedded basalt that has been dated at 1800 ± 13 (Miller et al., 2000). The Damtha Group itself has been bracketed with detrital zircon ages to be between ~1800 Ma and ~1600 Ma (McKenzie et al., 2011). Our samples are from an organic-rich black shale unit within this group, and were collected at N 29.599033°; E 80.194150°, north west of Pithoragarh, Uttarakhand.

The ~2.35 Ga Timeball Hill Formation, South Africa

The Timeball Hill Formation in the lower part of the Pretoria Group, Transvaal Supergroup of South Africa was deposited between the last two Paleoproterozoic glacial events, evidenced by the underlying diamictite in the Rooihoogte Formation, and the overlying Makganyene diamictite. This formation has a Re-Os date of 2316 ± 7 Ma (Hannah et al., 2004), with a precise isochron indicating minimal post-depositional mobilization of trace metals. Our samples are from the EBA-1 core, which was drilled near the town of Potchefstroom, outside of the metamorphic aureole of the Bushveld Complex (Coetzee et al., 2006). The Timeball Hill Formation also lacks a MIF-Sulfur signal, indicating deposition after a shift to pO_2 levels above 10^{-5} PAL (Bekker et al., 2004)

The ~ 2.5 Ga Mt. McRae Shale, Western Australia

The Mount McRae Shale was deposited in the Hamersley Basin of the Pilbara, northwestern Australia at ~ 2.5 Ga, based on a Re – Os age of 2501.1 ± 8.2 Ma from the middle part of the unit (~ 129m – 147m) (Kendall et al., 2015). The Mt. McRae is composed of well-preserved sediments accumulated in the basin during two depositional cycles, each beginning with a carbonate or siliciclastic turbidite and deepening upward into a shale or banded iron formation (Kaufman et al., 2007; Krapež et al., 2003). The Re-Os date and our samples are from the ABDP-9 core, drilled in 2004 as part of the Deep Time Drilling Project (DTDP) of the Astrobiology Drilling Program (ADP) collected as part of the Archean Biosphere Drilling Project (ABDP). Our samples are the same as those used for iron speciation and sulfur isotope analyses by (Reinhard et al., 2009) which show the formation was deposited under largely euxinic conditions. Again, very coherent Re-Os isochron systematics indicate minimal post-depositional mobility of metals.

The ~2.55 Mount Sylvia Formation, Western Australia

The Mount Sylvia Formation directly underlies the Mount McRae Shale, and these samples were also from the ADBP-9 core. The Wittenoom Formation lies just below the Mt. Sylvia and has provided a U-Pb zircon age of 2561 ± 8 Ma from a tuff (Nelson et al., 1999). This brackets the Mt. Sylvia between 2561 ± 8 Ma (Nelson et al., 1999) and 2501.1 ± 8.2 Ma (Anbar et al., 2007).

The ~2.7 Roy Hill Shale Member of the Jeerinah Formation, Western Australia

The Roy Hill Shale is the uppermost member of the Jeerinah Formation of the Fortescue Group of northwestern Australia. Our samples are from the AIDP-2 core drilled at Ripon hill and the AIDP-3 core drilled at Tunkawanna of the 2012 Agouron Institute Drilling Project. The Jeerinah formation has been dated at ~ 2.68 Ga based on two contemporaneous volcanoclastic samples that have yielded zircons with U-Pb ages of 2690 ± 16 Ma and 2684 ± 8 Ma (Arndt et al., 1991). See (French et al., 2015) for a full description of the core.

SI REFERENCES

Abbott, S. T., and Sweet, I. P., 2000, Tectonic control on third-order sequences in a siliciclastic ramp-style basin: an example from the Roper Superbasin (Mesoproterozoic), northern Australia: Australian Journal of Earth Sciences, v. 47, no. 3, p. 637-657.

Anbar, A. D., Duan, Y., Lyons, T. W., Arnold, G. L., Kendall, B., Creaser, R. A., Kaufman, A. J., Gordon, G. W., Scott, C., Garvin, J., and Buick, R., 2007, A Whiff of Oxygen Before the Great Oxidation Event?: Science, v. 317, no. 5846, p. 1903-1906.

Arndt, N. T., Nelson, D. R., Compston, W., Trendall, A. F., and Thorne, A. M., 1991, The age of the Fortescue Group, Hamersley Basin, Western Australia, from ion microprobe zircon U‐Pb results: Australian Journal of Earth Sciences, v. 38, no. 3, p. 261-281.

Bekker, A., Holland, H. D., Wang, P. L., Rumble, D., Stein, H. J., Hannah, J. L., Coetzee, L. L., and Beukes, N. J., 2004, Dating the rise of atmospheric oxygen: Nature, v. 427, no. 6970, p. 117-120.

Calver, C. R., 1998, Isotope stratigraphy of the Neoproterozoic Togari Group, Tasmania: Australian Journal of Earth Sciences, v. 45, no. 6, p. 865.

Calver, C. R., 2011, Neoproterozoic glacial deposits of Tasmania: Geological Society, London, Memoirs, v. 36, no. 1, p. 649-658.

Chuanming, Z., Guwei, X., McFadden, K., Shuhai, X., and Xunlai, Y., 2007, The diversification and extinction of Doushantuo-Pertatataka acritarchs in South China: causes and biostratigraphic significance: Geological Journal, v. 42, no. 3-4, p. 229-262.

Coetzee, L. L., Beukes, N. J., Gutzmer, J., and Kakegawa, T., 2006, Links of organic carbon cycling and burial to depositional depth gradients and establishment of a snowball Earth at 2.3Ga. Evidence from the Timeball Hill Formation,Transvaal Supergroup, South Africa: South African Journal of Geology, v. 109, no. 1-2, p. 109-122.

Condon, D., Zhu, M., Bowring, S., Wang, W., Yang, A., and Jin, Y., 2005, U-Pb Ages from the Neoproterozoic Doushantuo Formation, China: Science, v. 308, no. 5718, p. 95-98.

Crowe, S. A., Dossing, L. N., Beukes, N. J., Bau, M., Kruger, S. J., Frei, R., and Canfield, D. E., 2013, Atmospheric oxygenation three billion years ago: Nature, v. 501, no. 7468, p. 535-538.

Dehler, C. M., Elrick, M., Karlstrom, K. E., Smith, G. A., Crossey, L. J., and Timmons, J. M., 2001, Neoproterozoic Chuar Group (~800–742 Ma), Grand Canyon: a record of cyclic marine deposition during global cooling and supercontinent rifting: Sedimentary Geology, v. 141–142, p. 465-499.

Denyszyn, S. W., Halls, H. C., Davis, D. W., and Evans, D. A. D., 2009, Paleomagnetism and U–Pb geochronology of Franklin dykes in High Arctic Canada and Greenland: a revised age and paleomagnetic pole constraining block rotations in the Nares Strait region: Canadian Journal of Earth Sciences, v. 46, no. 9, p. 689-705.

469 Flannery, E. N., and George, S. C., 2014, Assessing the syngeneity and indigeneity of
470 hydrocarbons in the ~1.4 Ga Velkerri Formation, McArthur Basin, using slice
471 experiments: Organic Geochemistry, v. 77, p. 115-125.
472 Frei, R., Gaucher, C., Poulton, S. W., and Canfield, D. E., 2009, Fluctuations in
473 Precambrian atmospheric oxygenation recorded by chromium isotopes:
474 Nature, v. 461, no. 7261, p. 250-253.
475 French, K. L., Hallmann, C., Hope, J. M., Schoon, P. L., Zumberge, J. A., Hoshino, Y.,
476 Peters, C. A., George, S. C., Love, G. D., Brocks, J. J., Buick, R., and Summons, R.
477 E., 2015, Reappraisal of hydrocarbon biomarkers in Archean rocks:
478 Proceedings of the National Academy of Sciences, v. 112, no. 19, p. 5915-
479 5920.
480 Goldman, D., Mitchell, C. E., Bergström, S. M., Delano, J. W., and Tice, S., 1994, K-
481 bentonites and graptolite biostratigraphy in the Middle Ordovician of New
482 York State and Quebec: a new chronostratigraphic model: Palaios, p. 124-
483 143.
484 Gueguen, B., Reinhard, C. T., Algeo, T. J., Peterson, L. C., Nielsen, S. G., Wang, X., Rowe,
485 H., and Planavsky, N. J., 2016, The chromium isotope composition of reducing
486 and oxic marine sediments: Geochimica et Cosmochimica Acta, v. 184, p. 1-
487 19.
488 Hannah, J. L., Bekker, A., Stein, H. J., Markey, R. J., and Holland, H. D., 2004, Primitive
489 Os and 2316 Ma age for marine shale: implications for Paleoproterozoic
490 glacial events and the rise of atmospheric oxygen: Earth and Planetary
491 Science Letters, v. 225, no. 1–2, p. 43-52.
492 Holland, H. D., 2006, The oxygenation of the atmosphere and oceans: Philosophical
493 Transactions of the Royal Society of London B: Biological Sciences, v. 361, no.
494 1470, p. 903-915.
495 Hughes, N. C., Peng, S., O.N., B., Ahluwalia , A. D., Walia , S., Myrow, P. M., and Parcha ,
496 S. K., 2005, Cambrian biostratigraphy of the Tal Group, Lesser Himalaya,
497 India, and early Tsanglangpuan (late early Cambrian) trilobites from the
498 Nigali Dhar syncline: Geological Magazine, v. 142, no. 1, p. 57-80.
499 Illing, C. J., Hallmann, C., Miller, K. E., Summons, R. E., and Strauss, H., 2014, Airborne
500 hydrocarbon contamination from laboratory atmospheres: Organic
501 Geochemistry, v. 76, p. 26-38.
502 Jackson, G., and Iannelli, T., 1981, Rift-related cyclic sedimentation in the
503 Neohelikian Borden Basin, northern Baffin Island: Geological Survey of
504 Canada, Paper, p. 81-10.
505 Jackson, M. J., and Raiswell, R., 1991, Sedimentology and carbon-sulphur
506 geochemistry of the Velkerri Formation, a mid-Proterozoic potential oil
507 source in northern Australia: Precambrian Research, v. 54, no. 1, p. 81-108.
508 Johnston, D. T., Farquhar, J., Summons, R. E., Shen, Y., Kaufman, A. J., Masterson, A. L.,
509 and Canfield, D. E., 2008, Sulfur isotope biogeochemistry of the Proterozoic
510 McArthur Basin: Geochimica et Cosmochimica Acta, v. 72, no. 17, p. 4278-
511 4290.
512 Karlstrom, K. E., Bowring, S. A., Dehler, C. M., Knoll, A. H., Porter, S. M., Marais, D. J. D.,
513 Weil, A. B., Sharp, Z. D., Geissman, J. W., Elrick, M. B., Timmons, J. M., Crossey,
514 L. J., and Davidek, K. L., 2000, Chuar Group of the Grand Canyon: Record of

breakup of Rodinia, associated change in the global carbon cycle, and ecosystem expansion by 740 Ma: Geology, v. 28, no. 7, p. 619-622.

Kaufman, A. J., Johnston, D. T., Farquhar, J., Masterson, A. L., Lyons, T. W., Bates, S., Anbar, A. D., Arnold, G. L., Garvin, J., and Buick, R., 2007, Late Archean Biospheric Oxygenation and Atmospheric Evolution: Science, v. 317, no. 5846, p. 1900-1903.

Kendall, B., Creaser, R. A., Calver, C. R., Raub, T. D., and Evans, D. A. D., 2009a, Correlation of Sturtian diamictite successions in southern Australia and northwestern Tasmania by Re–Os black shale geochronology and the ambiguity of "Sturtian"-type diamictite–cap carbonate pairs as chronostratigraphic marker horizons: Precambrian Research, v. 172, no. 3–4, p. 301-310.

Kendall, B., Creaser, R. A., Gordon, G. W., and Anbar, A. D., 2009b, Re–Os and Mo isotope systematics of black shales from the Middle Proterozoic Velkerri and Wollogorang Formations, McArthur Basin, northern Australia: Geochimica et Cosmochimica Acta, v. 73, no. 9, p. 2534-2558.

Kendall, B., Creaser, R. A., Reinhard, C. T., Lyons, T. W., and Anbar, A. D., 2015, Transient episodes of mild environmental oxygenation and oxidative continental weathering during the late Archean: Science Advances, v. 1, no. 10.

Krapež, B., Barley, M. E., and Pickard, A. L., 2003, Hydrothermal and resedimented origins of the precursor sediments to banded iron formation: sedimentological evidence from the Early Palaeoproterozoic Brockman Supersequence of Western Australia: Sedimentology, v. 50, no. 5, p. 979-1011.

Lehmann, D., Brett, C. E., Cole, R., and Baird, G., 1995, Distal sedimentation in a peripheral foreland basin: Ordovician black shales and associated flysch of the western Taconic foreland, New York State and Ontario: Geological Society of America Bulletin, v. 107, no. 6, p. 708-724.

Liu, P., Yin, C., Gao, L., Tang, F., and Chen, S., 2009, New material of microfossils from the Ediacaran Doushantuo Formation in the Zhangcunping area, Yichang, Hubei Province and its zircon SHRIMP U-Pb age: Chinese Science Bulletin, v. 54, no. 6, p. 1058-1064.

Love, G. D., Grosjean, E., Stalvies, C., Fike, D. A., Grotzinger, J. P., Bradley, A. S., Kelly, A. E., Bhatia, M., Meredith, W., Snape, C. E., Bowring, S. A., Condon, D. J., and Summons, R. E., 2009, Fossil steroids record the appearance of Demospongiae during the Cryogenian period: Nature, v. 457, no. 7230, p. 718-U715.

Luo, G., Hallmann, C., Xie, S., Ruan, X., and Summons, R. E., 2015, Comparative microbial diversity and redox environments of black shale and stromatolite facies in the Mesoproterozoic Xiamaling Formation: Geochimica et Cosmochimica Acta, v. 151, p. 150-167.

Macdonald, F. A., Schmitz, M. D., Crowley, J. L., Roots, C. F., Jones, D. S., Maloof, A. C., Strauss, J. V., Cohen, P. A., Johnston, D. T., and Schrag, D. P., 2010, Calibrating the Cryogenian: Science, v. 327, no. 5970, p. 1241-1243.

560 McFadden, K. A., Huang, J., Chu, X., Jiang, G., Kaufman, A. J., Zhou, C., Yuan, X., and
561 Xiao, S., 2008, Pulsed oxidation and biological evolution in the Ediacaran
562 Doushantuo Formation: Proceedings of the National Academy of Sciences, v.
563 105, no. 9, p. 3197-3202.
564 McKenzie, N. R., Hughes, N. C., Myrow, P. M., Xiao, S., and Sharma, M., 2011,
565 Correlation of Precambrian–Cambrian sedimentary successions across
566 northern India and the utility of isotopic signatures of Himalayan
567 lithotectonic zones: Earth and Planetary Science Letters, v. 312, no. 3–4, p.
568 471-483.
569 Miller, C., Klötzli, U., Frank, W., Thöni, M., and Grasemann, B., 2000, Proterozoic
570 crustal evolution in the NW Himalaya (India) as recorded by circa 1.80 Ga
571 mafic and 1.84 Ga granitic magmatism: Precambrian Research, v. 103, no. 3–
572 4, p. 191-206.
573 Nelson, D. R., Trendall, A. F., and Altermann, W., 1999, Chronological correlations
574 between the Pilbara and Kaapvaal cratons: Precambrian Research, v. 97, no.
575 3–4, p. 165-189.
576 Page, R. W., Jackson, M. J., and Krassay, A. A., 2000, Constraining sequence
577 stratigraphy in north Australian basins: SHRIMP U–Pb zircon geochronology
578 between Mt Isa and McArthur River*: Australian Journal of Earth Sciences, v.
579 47, no. 3, p. 431-459.
580 Planavsky, N. J., Cole, D. B., Reinhard, C. T., Diamond, C., Love, G. D., Luo, G., Zhang, S.,
581 Konhauser, K. O., and Lyons, T. W., 2016, No evidence for high atmospheric
582 oxygen levels 1,400 million years ago: Proceedings of the National Academy
583 of Sciences.
584 Planavsky, N. J., McGoldrick, P., Scott, C. T., Li, C., Reinhard, C. T., Kelly, A. E., Chu, X.,
585 Bekker, A., Love, G. D., and Lyons, T. W., 2011, Widespread iron-rich
586 conditions in the mid-Proterozoic ocean: Nature, v. 477, no. 7365, p. 448-451.
587 Planavsky, N. J., Reinhard, C. T., Wang, X., Thomson, D., McGoldrick, P., Rainbird, R.
588 H., Johnson, T., Fischer, W. W., and Lyons, T. W., 2014, Low Mid-Proterozoic
589 atmospheric oxygen levels and the delayed rise of animals: Science, v. 346,
590 no. 6209, p. 635-638.
591 Porter, S. M., and Knoll, A. H., 2000, Testate amoebae in the Neoproterozoic Era:
592 evidence from vase-shaped microfossils in the Chuar Group, Grand Canyon:
593 Journal Information, v. 26, no. 3.
594 Reinhard, C. T., Planavsky, N. J., Wang, X., Fischer, W. W., Johnson, T. M., and Lyons, T.
595 W., 2014, The isotopic composition of authigenic chromium in anoxic marine
596 sediments: A case study from the Cariaco Basin: Earth and Planetary Science
597 Letters, v. 407, no. 0, p. 9-18.
598 Reinhard, C. T., Raiswell, R., Scott, C., Anbar, A. D., and Lyons, T. W., 2009, A Late
599 Archean Sulfidic Sea Stimulated by Early Oxidative Weathering of the
600 Continents: Science, v. 326, no. 5953, p. 713-716.
601 Riedman, L. A., Porter, S. M., Halverson, G. P., Hurtgen, M. T., and Junium, C. K., 2014,
602 Organic-walled microfossil assemblages from glacial and interglacial
603 Neoproterozoic units of Australia and Svalbard: Geology, v. 42, no. 11, p.
604 1011-1014.
605 Ruedemann, R., 1908, Graptolites of New York, New York Education Department.

606 Rye, R., and Holland, H. D., 1998, Paleosols and the evolution of atmospheric oxygen:
607 a critical review: American journal of science, v. 298, no. 8, p. 621-672.
608 Sahoo, S. K., Planavsky, N. J., Jiang, G., Kendall, B., Owens, J. D., Wang, X., Shi, X., Anbar,
609 A. D., and Lyons, T. W., 2016, Oceanic oxygenation events in the anoxic
610 Ediacaran ocean: Geobiology, p. n/a-n/a.
611 Sahoo, S. K., Planavsky, N. J., Kendall, B., Wang, X., Shi, X., Scott, C., Anbar, A. D., Lyons,
612 T. W., and Jiang, G., 2012, Ocean oxygenation in the wake of the Marinoan
613 glaciation: Nature, v. 489, no. 7417, p. 546-549.
614 Scheiderich, K., Amini, M., Holmden, C., and Francois, R., 2015, Global variability of
615 chromium isotopes in seawater demonstrated by Pacific, Atlantic, and Arctic
616 Ocean samples: Earth and Planetary Science Letters, v. 423, p. 87-97.
617 Schoenberg, R., Zink, S., Staubwasser, M., and von Blanckenburg, F., 2008, The stable
618 Cr isotope inventory of solid Earth reservoirs determined by double spike
619 MC-ICP-MS: Chemical Geology, v. 249, no. 3–4, p. 294-306.
620 Sheldon, N. D., 2013, Causes and consequences of low atmospheric pCO2 in the Late
621 Mesoproterozoic: Chemical Geology, v. 362, p. 224-231.
622 Siebert, C., Nagler, T. F., and Kramers, J. D., 2001, Determination of molybdenum
623 isotope fractionation by double-spike multicollector inductively coupled
624 plasma mass spectrometry: Geochemistry Geophysics Geosystems, v. 2, p.
625 1032.
626 Singh, S. K., Trivedi, J. R., and Krishnaswami, S., 1999, Re-Os isotope systematics in
627 black shales from the Lesser Himalaya: their chronology and role in the
628 187Os/188Os evolution of seawater: Geochimica et Cosmochimica Acta, v.
629 63, no. 16, p. 2381-2392.
630 Su, W., Zhang, S., Huff, W. D., Li, H., Ettensohn, F. R., Chen, X., Yang, H., Han, Y., Song,
631 B., and Santosh, M., 2008, SHRIMP U–Pb ages of K-bentonite beds in the
632 Xiamaling Formation: Implications for revised subdivision of the Meso- to
633 Neoproterozoic history of the North China Craton: Gondwana Research, v. 14,
634 no. 3, p. 543-553.
635 Turner, E. C., and Kamber, B. S., 2012, Arctic Bay Formation, Borden Basin, Nunavut
636 (Canada): Basin evolution, black shale, and dissolved metal systematics in the
637 Mesoproterozoic ocean: Precambrian Research, v. 208–211, no. 0, p. 1-18.
638 Zhang, S., Wang, X., Wang, H., Bjerrum, C. J., Hammarlund, E. U., Costa, M. M.,
639 Connelly, J. N., Zhang, B., Su, J., and Canfield, D. E., 2016a, Sufficient oxygen for
640 animal respiration 1,400 million years ago: Proceedings of the National
641 Academy of Sciences.
642 Zhang, S., Wang, X., Wang, H., Bjerrum, C. J., Hammarlund, E. U., Dahl, T. W., and
643 Canfield, D. E., 2016b, Reply to Planavsky et al.: Strong evidence for high
644 atmospheric oxygen levels 1,400 million years ago: Proceedings of the
645 National Academy of Sciences.
646 Zhu, M., Zhang, J., and Yang, A., 2007, Integrated Ediacaran (Sinian)
647 chronostratigraphy of South China: Palaeogeography, Palaeoclimatology,
648 Palaeoecology, v. 254, no. 1–2, p. 7-61.
649
650

SI Table 1. All data reported in this study

SAMPLES				BULK SUMMARY					LEACH SUMMARY				
Group/Formation	Age	Section/Core	Strat Height/Core Depth (m)	[Ti] ppm bulk	[Cr] ppm bulk	Cr/Ti (Bulk)	(‰) $\delta^{53/52}Cr_{bulk}$	2se	[Ti] ppm leach	[Cr] ppm leach	Cr/Ti (Leach)	(‰) $\delta^{53/52}Cr_{leach}$	2se
Doldgeville Fm.	450		DD7	747.728	22.393	0.028	0.28	0.05					
Doldgeville Fm.	450		DD8	1070.415	21.925	0.030	0.34	0.04					
Doldgeville Fm.	450		DD9	1069.173	23.837	0.020	0.58	0.05					
Doldgeville Fm.	450		DD10	837.866	23.773	0.022	0.49	0.05					
Tal Group	550	DCIT2	14.2	2357.601	72.108	0.031	0.23	0.04					
Tal Group	550	DCIT2	17.7	1919.147	91.590	0.048	0.46	0.05					
Tal Group	550	DCIT2	19.1	2314.629	107.787	0.047	0.55	0.05					
Tal Group	550	DCIT2	23.2	2156.185	101.260	0.047	0.59	0.04					
Tal Group	550	DCIT2	40.2	1408.851	92.433	0.066	0.16	0.03					
Tal Group	550	DCIT2	43.8	1565.365	104.571	0.067	0.53	0.04					
Tal Group	550	DCIT2	52	2560.561	83.796	0.033	0.17	0.05					
Doushantou	630	WH09	6	3812.601	54.733	0.014	-0.13	0.04					
Doushantou	630	WH09	5.4	3409.097	49.631	0.015	-0.11	0.03					
Doushantou	630	WH09	5.6	2774.013	39.836	0.014	-0.16	0.03					
Doushantou	630	WH09	6.5	3645.168	53.410	0.015	-0.04	0.03					
Doushantou	630	WH09	6.8	4109.399	57.123	0.014	-0.05	0.03					
Doushantou	630	WH09	8.6	3823.384	50.676	0.013	-0.10	0.03					
Tongari Group	640	Forest-1	805.85	14297.507	287.591	0.020	-0.16	0.03					
Tongari Group	640	Forest-1	830.7	4345.014	76.664	0.018	0.10	0.03					
Tongari Group	640	Forest-1	880.7	6581.705	105.093	0.016	0.14	0.03					
Tongari Group	640	Forest-1	914.9	4187.104	65.277	0.016	0.16	0.04					
Tongari Group	640	Forest-1	939.5	5045.628	60.103	0.012	0.12	0.03					
Tongari Group	800	Forest-1	1045.4	319.269	28.493	0.089	0.09	0.03					
Tongari Group	800	Forest-1	1024	445.510	47.750	0.107	0.23	0.04					
Tongari Group	800	Forest-1	1057	123.048	13.935	0.113	0.24	0.05					
Chuar	740	Walcott	WAL-4	2588.815	86.624	0.033	0.70	0.05					
Chuar	740	Walcott	WAL-5	2749.400	93.748	0.034	0.73	0.05					
Chuar	740	Walcott	WAL-6	3116.619	101.739	0.033	0.68	0.05					
Chuar	740	Walcott	3	4440.386	173.997	0.039	0.70	0.05					
Chuar	740	Walcott	8	4747.836	101.996	0.021	0.58	0.04					
Chuar	740	Walcott	19.2	4882.299	99.733	0.020	0.62	0.03					
Chuar	740	Walcott	27.1	5207.908	143.155	0.027	0.73	0.03					
Chuar	740	Walcott	30	5355.931	126.432	0.024	0.60	0.03					

SI Table 1. All data reported in this study

SAMPLES				BULK SUMMARY					LEACH SUMMARY				
Group/Formation	Age	Section/Core	Strat Height/Core Depth (m)	[Ti] ppm bulk	[Cr] ppm bulk	Cr/Ti (Bulk)	(‰) $\delta^{53/52}Cr_{bulk}$	2se	[Ti] ppm leach	[Cr] ppm leach	Cr/Ti (Leach)	(‰) $\delta^{53/52}Cr_{leach}$	2se
Chuar	740	Walcott	37	3249.333	67.745	0.021	0.52	0.03					
Chuar	740	Awatubi	3	6757.936	112.336	0.017	0.15	0.03					
Simla	840	Theog-Matiana (	0	2079.064	68.174	0.033	-0.04	0.04					
Simla	840	Theog-Matiana (	19.7	2509.924	69.302	0.028	0.04	0.04					
Simla	840	Theog-Matiana (	29	1808.765	65.917	0.036	0.08	0.04					
Simla	840	Theog-Matiana (	64.5	1253.338	62.077	0.050	0.10	0.05					
Simla	840	Tons Valley (DCI	2	1264.277	28.362	0.022	0.16	0.05					
Simla	840	Tons Valley (DCI	3	1414.430	64.457	0.046	0.09	0.05					
Simla	840	YR02		2996.548	71.928	0.024	-0.09	0.03					
Simla	840	SB01		3865.415	68.807	0.018	-0.08	0.03					
Arctic Bay	1.1	PWC1405	636.5	4229.519	88.078	0.021	-0.07	0.02	0.681	0.060	11.35	-0.14	0.02
Arctic Bay	1.1	PWC1405	600.5	3700.800	81.571	0.022	-0.12	0.02	1.020	0.047	21.58	-0.19	0.02
Arctic Bay	1.1	PWC1405	479.8						0.382	0.159	2.41	-0.14	0.02
Arctic Bay	1.1	PWC1405	458.6						0.355	0.137	2.60	-0.08	0.02
Arctic Bay	1.1	PWC1405	388						0.177	0.139	1.27	-0.18	0.02
Arctic Bay	1.1	PWC1405	340						0.140	0.114	1.23	-0.17	0.02
Arctic Bay	1.1	PWC1405	257.5						0.157	0.185	0.85	-0.15	0.02
Arctic Bay	1.1	PWC1405	216						0.715	0.268	2.67	-0.20	0.02
Arctic Bay	1.1	PWC1405	110.5						0.186	0.259	0.72	-0.18	0.02
Arctic Bay	1.1	PWC1405	74	4854.266	85.378	0.018	-0.14	0.02	0.119	0.313	0.38	-0.19	0.02
Arctic Bay	1.1	PWC1405	45.1						0.245	0.222	1.10	-0.17	0.02
Arctic Bay	1.1	T1413	282.2						0.355	0.156	2.28	0.07	0.02
Arctic Bay	1.1	T1413	226.5	2331.868	44.353	0.019	0.08	0.02					
Arctic Bay	1.1	T1413	204.5	2542.545	48.817	0.019	0.01	0.02	0.379	0.085	4.46	-0.02	0.02
Arctic Bay	1.1	T1413	196.9						0.341	0.063	5.44	-0.03	
Arctic Bay	1.1	T1413	192.5	2452.714	46.338	0.019	0.06	0.02					
Arctic Bay	1.1	T1413	187.1	2369.385	51.829	0.022	0.07	0.02					
Arctic Bay	1.1	T1413	166.4	2808.037	57.927	0.021	0.01	0.02					
Arctic Bay	1.1	T1413	149.4	3629.496	80.891	0.022	-0.07	0.02					
Arctic Bay	1.1	T1413	129.7	3925.057	93.181	0.024	-0.10	0.02					
Arctic Bay	1.1	T1413	126.5	4292.707	101.694	0.024	-0.10	0.02					
Arctic Bay	1.1	T1413	112.3	4350.013	88.174	0.020	-0.13	0.02					
Arctic Bay	1.1	T1413	105.7	2579.204	50.859	0.020	-0.13	0.02					

SI Table 1. All data reported in this study

SAMPLES				BULK SUMMARY					LEACH SUMMARY				
Group/Formation	Age	Section/Core	Strat Height/Core Depth (m)	[Ti] ppm bulk	[Cr] ppm bulk	Cr/Ti (Bulk)	(‰) $\delta^{53/52}Cr_{bulk}$	2se	[Ti] ppm leach	[Cr] ppm leach	Cr/Ti (Leach)	(‰) $\delta^{53/52}Cr_{leach}$	2se
Arctic Bay	1.1	T1413	94.9	5231.976	90.570	0.017	-0.12	0.02	0.704	0.104	6.80	-0.17	0.03
Arctic Bay	1.1	T1413	76.4	3234.729	60.875	0.019	-0.05	0.02					
Arctic Bay	1.1	MB1401	6.4	4238.634	81.058	0.019	-0.09	0.02	1.601	0.162	9.87	-0.18	0.02
Arctic Bay	1.1	MB1401	10	4241.783	90.236	0.021	-0.04	0.01	2.178	0.174	12.51	-0.10	0.02
Arctic Bay	1.1	MB1401	16	3540.400	78.370	0.022	-0.03	0.02	0.295	0.261	1.13	-0.20	0.02
Arctic Bay	1.1	MB1401	21.4	3894.246	78.772	0.020	0.09	0.02	2.953	0.177	16.67	-0.01	0.03
Arctic Bay	1.1	MB1401	31	3592.165	81.642	0.023	-0.11	0.02	0.356	0.033	10.71	-0.14	0.02
Arctic Bay	1.1	MB1401	40.5	3566.086	77.256	0.022	-0.03	0.02	0.605	0.091	6.65	-0.09	0.02
Arctic Bay	1.1	MB1401	66	3622.158	81.228	0.022	-0.09	0.02	0.316	0.165	1.92	-0.15	0.02
Arctic Bay	1.1	MB1401	75	4003.757	87.439	0.022	-0.10	0.02	0.180	0.149	1.21	-0.13	0.02
Arctic Bay	1.1	MB1401	91	5038.352	90.861	0.018	-0.13	0.01	0.383	0.149	2.58	-0.14	0.03
Arctic Bay	1.1	MB1401	102.8	2708.608	58.678	0.022	0.03	0.02	0.354	0.258	1.37	0.06	0.02
Arctic Bay	1.1	MB1401	113.7	3437.189	71.484	0.021	-0.09	0.02					
Arctic Bay	1.1	MB1401	441.5	3816.692	76.720	0.020	-0.16	0.02					
Xiamaling	1.38	XQ1	12	3731.938	51.802	0.014	-0.05	0.03					
Xiamaling	1.38	XQ1	20	3801.174	51.413	0.014	-0.03	0.02					
Xiamaling	1.38	XQ1	27	2533.712	42.861	0.017	-0.09	0.02					
Xiamaling	1.38	XQ1	32	4151.934	65.429	0.016	-0.04	0.02					
Xiamaling	1.38	XQ1	37	2979.989	45.205	0.015	0.17	0.02					
Xiamaling	1.38	XQ1	68	4928.372	68.035	0.014	-0.19	0.03					
Velkerri	1.4	Urapunga - 4	36.98-137.05						3.126	0.121	25.93	-0.10	0.02
Velkerri	1.4	Urapunga - 4	37.19-137.26	2220.237	38.534	0.017	-0.14	0.02	2.902	0.113	25.64	-0.07	0.02
Velkerri	1.4	Urapunga - 4	37.26-137.33	2417.095	40.933	0.017	-0.01	0.02	3.146	0.122	25.76	-0.15	0.02
Velkerri	1.4	Urapunga - 4	37.46-137.52	2463.611	44.551	0.018	0.05	0.02	3.209	0.118	27.27	-0.07	0.03
Velkerri	1.4	Urapunga - 4	37.75-137.79						2.728	0.117	23.32	-0.11	0.03
Velkerri	1.4	Urapunga - 4	37.84-137.89						2.744	0.109	25.18	-0.13	0.02
Velkerri	1.4	Urapunga - 4	25.71-325.78	3180.169	39.217	0.012	-0.13	0.02					
Velkerri	1.4	Urapunga - 4	26.20-326.28	3104.687	41.168	0.013	-0.09	0.02	1.273	0.111	11.44	-0.16	0.02
Velkerri	1.4	Urapunga - 4	26.42-326.48	3301.915	40.603	0.012	-0.14	0.03	1.173	0.081	14.43	-0.18	0.02
Velkerri	1.4	Urapunga - 4	26.48-346.55	3138.317	39.846	0.013	-0.14	0.02	1.380	0.106	12.98	-0.17	0.02
Velkerri	1.4	Urapunga - 4	26.62-326.69	2867.082	36.147	0.013	-0.13	0.02	1.459	0.143	10.23	-0.15	0.01
Barney Creek	1.65	MY4	61.5	2674.393	38.655	0.014	-0.17	0.02					
Barney Creek	1.65	MY4	77.5	2231.855	35.315	0.016	-0.34	0.02					

SI Table 1. All data reported in this study

SAMPLES				BULK SUMMARY					LEACH SUMMARY				
Group/Formation	Age	Section/Core	Strat Height/Core Depth (m)	[Ti] ppm bulk	[Cr] ppm bulk	Cr/Ti (Bulk)	(‰) $\delta^{53/52}Cr_{bulk}$	2se	[Ti] ppm leach	[Cr] ppm leach	Cr/Ti (Leach)	(‰) $\delta^{53/52}Cr_{leach}$	2se
Barney Creek	1.65	MY4	87.8	907.725	14.871	0.016	-0.11	0.03					
Barney Creek	1.65	MY4	100.6	724.853	17.040	0.024	-0.14	0.02					
Barney Creek	1.65	MY4	105.7	656.764	10.874	0.017	-0.13	0.02					
Barney Creek	1.65	MY4	125.2	1123.183	16.595	0.015	-0.09	0.02					
Barney Creek	1.65	MY4	175	1210.676	14.531	0.012	-0.14	0.02					
Barney Creek	1.65	MY4	198	2114.587	28.506	0.013	-0.14	0.02					
Barney Creek	1.65	MY4	228	2543.966	42.878	0.017	-0.11	0.02					
Barney Creek	1.65	MY4	233.8	267.256	7.575	0.028	-0.14	0.02					
Mt. Les Siltstone	1.65	WFDD 84	103.5	2288.071	36.074	0.016	-0.10	0.02					
Mt. Les Siltstone	1.65	WFDD 84	115.2	2096.983	31.783	0.015	-0.17	0.02					
Mt. Les Siltstone	1.65	WFDD 84	156.5	2335.265	20.301	0.009	-0.28	0.03					
Mt. Les Siltstone	1.65	WFDD 84	97.8	770.411	12.634	0.016	-0.08	0.03					
Lady Lorreta	1.65	LA64	116	2723.207	49.295	0.018	-0.18	0.02					
Lady Lorreta	1.65	LA64	146	2421.485	44.310	0.018	-0.19	0.02					
Lady Lorreta	1.65	LA64	289.8	1118.348	46.858	0.042	-0.18	0.01					
Lady Lorreta	1.65	LA64	301	2112.641	40.462	0.019	-0.20	0.02					
Lady Lorreta	1.65	LA64	543	1165.782	24.720	0.021	-0.17	0.03					
Lady Lorreta	1.65	LA64	564	2393.308	36.094	0.015	-0.23	0.03					
Lady Lorreta	1.65	LA64	600.5	2977.723	51.693	0.017	-0.20	0.02					
Damtha	1.7	CHBS1		3167.304	51.839	0.016	-0.15	0.02					
Damtha	1.7	CHBS2		3339.714	54.911	0.016	-0.06	0.02					
Damtha	1.7	CHBS3		3375.503	57.190	0.017	-0.09	0.02					
Damtha	1.7	CHBS4		3518.432	58.090	0.017	-0.14	0.03					
Damtha	1.7	CHBS7		3478.110	58.417	0.017	-0.13	0.02					
Timeball Hill	2.32	EBA-1	118	3456.78535	67.08947	0.019	-0.10	0.05					
Timeball Hill	2.32	EBA-1	125	5408.15558	155.6448	0.029	-0.27	0.05					
Timeball Hill	2.32	EBA-1	15	3762.14136	124.6515	0.033	-0.03	0.05					
Timeball Hill	2.32	EBA-1	27	2206.06293	145.2145	0.066	-0.15	0.04					
Timeball Hill	2.32	EBA-1	41	2818.45887	155.9421	0.055	-0.12	0.04					
Timeball Hill	2.32	EBA-1	51	1978.16557	173.7198	0.088	-0.10	0.05					
Timeball Hill	2.32	EBA-1	68	2334.41426	160.851	0.069	-0.09	0.05					
Timeball Hill	2.32	EBA-1	77	3361.37516	172.3536	0.051	-0.17	0.05					
Timeball Hill	2.32	EBA-1	92	4780.43282	147.0887	0.031	-0.16	0.05					

SI Table 1. All data reported in this study

SAMPLES				BULK SUMMARY					LEACH SUMMARY				
Group/Formation	Age	Section/Core	Strat Height/Core Depth (m)	[Ti] ppm bulk	[Cr] ppm bulk	Cr/Ti (Bulk)	(‰) $\delta^{53/52}Cr_{bulk}$	2se	[Ti] ppm leach	[Cr] ppm leach	Cr/Ti (Leach)	(‰) $\delta^{53/52}Cr_{leach}$	2se
Roy Hill Shale mbr.	2.7	AIDP-2	299.24	4982.359	217.952	0.044	-0.12	0.02	0.168	0.209	1.24	-0.16	0.04
Roy Hill Shale mbr.	2.7	AIDP-2	302.11	5631.226	193.487	0.034	-0.16	0.02					
Roy Hill Shale mbr.	2.7	AIDP-2	306.05	4318.356	197.746	0.046	-0.13	0.03					
Roy Hill Shale mbr.	2.7	AIDP-2	309.12	4987.888	151.370	0.030	-0.14	0.02	0.152	0.182	1.20	-0.15	0.04
Roy Hill Shale mbr.	2.7	AIDP-2	311.15	7170.455	232.353	0.032	-0.11	0.03					
Roy Hill Shale mbr.	2.7	AIDP-2	315.67	2748.328	92.178	0.034	-0.17	0.03					
Roy Hill Shale mbr.	2.7	AIDP-2	319.89	1681.708	66.574	0.040	-0.09	0.03	0.065	0.054	0.83	-0.07	0.06
Roy Hill Shale mbr.	2.7	AIDP-2	322.31	2536.957	80.304	0.032	-0.08	0.07					
Roy Hill Shale mbr.	2.7	AIDP-2	324.85	2851.824	91.609	0.032	-0.10	0.05					
Roy Hill Shale mbr.	2.7	AIDP-2	328.46	2582.423	78.784	0.031	-0.13	0.03					
Roy Hill Shale mbr.	2.7	AIDP-2	330.6	4251.595	138.000	0.032	-0.14	0.03					
Roy Hill Shale mbr.	2.7	AIDP-2	332.52	2923.435	74.646	0.026	-0.07	0.03	0.121	0.142	1.18	-0.14	0.04
Roy Hill Shale mbr.	2.7	AIDP-2	338.85	3072.472	66.031	0.021	-0.15	0.04	0.123	0.085	0.69	-0.12	0.04
Roy Hill Shale mbr.	2.7	AIDP-2	342.74	3809.648	140.294	0.037	-0.02	0.04					
Roy Hill Shale mbr.	2.7	AIDP-2	344.99	5451.463	127.106	0.023	-0.11	0.04	0.027	0.012	0.46	-0.17	0.05
Roy Hill Shale mbr.	2.7	AIDP-2	352.56	4206.659	224.595	0.053	-0.14	0.03					
Roy Hill Shale mbr.	2.7	AIDP-2	354.66	4025.419	223.573	0.056	-0.14	0.04	0.031	0.051	1.64	-0.07	0.04
Roy Hill Shale mbr.	2.7	AIDP-2	358.09	4326.334	225.073	0.052	-0.11	0.03					
Roy Hill Shale mbr.	2.7	AIDP-2	360.39	4366.412	214.440	0.049	-0.11	0.04	0.028	0.022	0.78	-0.16	0.04
Roy Hill Shale mbr.	2.7	AIDP-2	363.04	4100.593	196.869	0.048	-0.13	0.05					
Roy Hill Shale mbr.	2.7	AIDP-2	366.34	3932.959	213.699	0.054	-0.14	0.03					
Roy Hill Shale mbr.	2.7	AIDP-2	369.05	4071.647	190.335	0.047	-0.16	0.04					
Roy Hill Shale mbr.	2.7	AIDP-2	370.69	4390.649	235.144	0.054	-0.13	0.04					
Roy Hill Shale mbr.	2.7	AIDP-2	371.54	4207.265	216.423	0.051	-0.13	0.03					
Roy Hill Shale mbr.	2.7	AIDP-2	374.04	3747.572	204.668	0.055	-0.12	0.03	0.124	0.207	1.67	-0.08	0.04
Roy Hill Shale mbr.	2.7	AIDP-2	377.05	4328.696	194.204	0.045	-0.15	0.06					
Roy Hill Shale mbr.	2.7	AIDP-2	382.76	3346.923	152.319	0.046	-0.12	0.04					
Roy Hill Shale mbr.	2.7	AIDP-3	68.22	5515.772	318.017	0.058	-0.07	0.03	0.068	0.064	0.94	-0.15	0.04
Roy Hill Shale mbr.	2.7	AIDP-3	71.22	4624.300	200.026	0.043	-0.11	0.04					
Roy Hill Shale mbr.	2.7	AIDP-3	79.78	4057.190	173.278	0.043	-0.09	0.04	0.090	0.037	0.41	-0.08	0.04
Roy Hill Shale mbr.	2.7	AIDP-3	91.67	2896.739	108.905	0.038	-0.11	0.04	0.044	0.010	0.23	-0.02	0.04
Roy Hill Shale mbr.	2.7	AIDP-3	95.92	2755.535	116.975	0.042	-0.11	0.04	0.067	0.036	0.53	-0.13	0.04
Roy Hill Shale mbr.	2.7	AIDP-3	104.5	1448.687	102.467	0.071	-0.13	0.08	0.054	0.109	2.02	-0.07	0.04

SI Table 1. All data reported in this study

SAMPLES				BULK SUMMARY					LEACH SUMMARY				
Group/Formation	Age	Section/Core	Strat Height/Core Depth (m)	[Ti] ppm bulk	[Cr] ppm bulk	Cr/Ti (Bulk)	(‰) $\delta^{53/52}Cr_{bulk}$	2se	[Ti] ppm leach	[Cr] ppm leach	Cr/Ti (Leach)	(‰) $\delta^{53/52}Cr_{leach}$	2se
Roy Hill Shale mbr.	2.7	AIDP-3	107.18	3369.438	241.434	0.072	-0.11	0.09	0.141	0.304	2.15	-0.08	0.04
Roy Hill Shale mbr.	2.7	AIDP-3	109.9	2242.391	123.979	0.055	-0.13	0.04	0.194	0.303	1.56	-0.10	0.04
Roy Hill Shale mbr.	2.7	AIDP-3	115.83	1923.359	173.856	0.090	-0.10	0.04	0.163	0.371	2.27	-0.05	0.04
Roy Hill Shale mbr.	2.7	AIDP-3	120.4	2210.142	243.093	0.110	0.03	0.05	0.172	0.431	2.50	-0.07	0.04
Roy Hill Shale mbr.	2.7	AIDP-3	131.31	5328.911	266.657	0.050	-0.10	0.04	0.177	0.360	2.03	-0.05	0.04
Roy Hill Shale mbr.	2.7	AIDP-3	134.13	2852.141	284.891	0.100	0.05	0.04	0.175	0.385	2.21	-0.07	0.04
Roy Hill Shale mbr.	2.7	AIDP-3	139.55	4199.722	303.139	0.072	-0.02	0.04					
Roy Hill Shale mbr.	2.7	AIDP-3	142.04	4561.332	299.600	0.066	-0.12	0.03	0.228	0.517	2.27	-0.08	0.04
Roy Hill Shale mbr.	2.7	AIDP-3	145.77	2400.496	255.230	0.106	-0.15	0.03	0.243	0.591	2.43	-0.10	0.04
Roy Hill Shale mbr.	2.7	AIDP-3	155.75	3297.167	281.920	0.086	-0.16	0.03					
Roy Hill Shale mbr.	2.7	AIDP-3	161.62	4223.521	340.450	0.081	-0.21	0.03					
Roy Hill Shale mbr.	2.7	AIDP-3	165.74	2908.862	206.060	0.071	-0.19	0.03					
Roy Hill Shale mbr.	2.7	AIDP-3	179.11	4732.967	292.310	0.062	-0.23	0.03	0.188	0.264	1.40	-0.12	0.04
Roy Hill Shale mbr.	2.7	AIDP-3	189.55	5324.270	238.070	0.045	-0.26	0.03					
Mt. McRae Shale	2.5	ABDP-9	113.46	3648.942	91.290	0.025	-0.15	0.04	0.215	0.084	0.39	-0.08	0.04
Mt. McRae Shale	2.5	ABDP-9	119.24	1302.225	36.660	0.028	-0.08	0.01					
Mt. McRae Shale	2.5	ABDP-9	126.15	3988.063	126.500	0.032	-0.19	0.03					
Mt. McRae Shale	2.5	ABDP-9	128.17	4544.221	150.300	0.033	-0.10	0.01	0.230	0.191	0.83	-0.08	0.04
Mt. McRae Shale	2.5	ABDP-9	130.06	4476.397	182.200	0.041	-0.17	0.03					
Mt. McRae Shale	2.5	ABDP-9	135.58	2183.939	51.590	0.024	0.01	0.07	0.190	0.087	0.46	-0.10	0.04
Mt. McRae Shale	2.5	ABDP-9	137.31	2645.144	70.730	0.027	-0.12	0.04					
Mt. McRae Shale	2.5	ABDP-9	137.96	2807.922	75.540	0.027	-0.23	0.02					
Mt. McRae Shale	2.5	ABDP-9	139.01	2767.227	73.000	0.026	-0.10	0.04	0.112	0.039	0.35	-0.09	0.04
Mt. McRae Shale	2.5	ABDP-9	139.97	3581.118	95.240	0.027	-0.08	0.01					
Mt. McRae Shale	2.5	ABDP-9	140.5	3608.247	126.200	0.035	-0.11	0.04					
Mt. McRae Shale	2.5	ABDP-9	141.72	3621.812	95.680	0.026	-0.15	0.03	0.269	0.088	0.33	-0.13	0.04
Mt. McRae Shale	2.5	ABDP-9	142.6	2156.810	68.820	0.032	-0.19	0.04					
Mt. McRae Shale	2.5	ABDP-9	144.36	2278.893	59.500	0.026	-0.09	0.04					
Mt. McRae Shale	2.5	ABDP-9	146.45	2618.014	66.810	0.026	-0.02	0.04	0.215	0.198	0.92	0.02	0.04
Mt. McRae Shale	2.5	ABDP-9	149.3	3147.043	71.260	0.023	-0.01	0.01					
Mt. McRae Shale	2.5	ABDP-9	153.18	2509.495	48.450	0.019	-0.10	0.01					
Mt. McRae Shale	2.5	ABDP-9	157.8	3309.821	98.670	0.030	-0.13	0.04					
Mt. McRae Shale	2.5	ABDP-9	167.76	1342.919	28.030	0.021	-0.10	0.04	0.515	0.216	0.42	-0.06	0.04

SI Table 1. All data reported in this study

SAMPLES				BULK SUMMARY					LEACH SUMMARY				
Group/Formation	Age	Section/Core	Strat Height/Core Depth (m)	[Ti] ppm bulk	[Cr] ppm bulk	Cr/Ti (Bulk)	(‰) $\delta^{53/52}Cr_{bulk}$	2se	[Ti] ppm leach	[Cr] ppm leach	Cr/Ti (Leach)	(‰) $\delta^{53/52}Cr_{leach}$	2se
Mt. Sylvia	2.55	ABDP-9	199.93	3662.510	130.924	0.036	-0.09	0.04					
Mt. Sylvia	2.55	ABDP-9	231.95	3126.700	106.243	0.034	-0.08	0.05					
Mt. Sylvia	2.55	ABDP-9	239.09	4467.410	180.692	0.040	-0.09	0.04					
Mt. Sylvia	2.55	ABDP-9	246.62	3800.870	161.954	0.043	-0.08	0.04					

SI Table 1. All data reported in this study

		ERRORS		
2 RMS Duplicates		**Nod A-1**		**BHVO-2**
0.062	Mean	0.07	Mean	-0.12
	2SD	0.08	2SD	0.06

SI Table 1. All data reported in this study

	ERRORS	
2 RMS Duplicates	**Nod A-1**	**BHVO-2**

SI Table 1. All data reported in this study

	ERRORS	
2 RMS Duplicates	**Nod A-1**	**BHVO-2**

SI Table 1. All data reported in this study

	ERRORS	
2 RMS Duplicates	**Nod A-1**	**BHVO-2**

SI Table 1. All data reported in this study

	ERRORS	
2 RMS Duplicates	**Nod A-1**	**BHVO-2**

SI Table 1. All data reported in this study

	ERRORS	
2 RMS Duplicates	**Nod A-1**	**BHVO-2**

SI Table 1. All data reported in this study

	ERRORS	
2 RMS Duplicates	**Nod A-1**	**BHVO-2**

SI Table 2. All Cr isotope data plotted on Figure 2 (main text)

SHALE/SILICICLASTIC				
Formation	**Age (Ga)**	**(‰) $\delta^{53/52}Cr_{bulk}$**	**2se**	**Reference**
Peru margin	0	0.57	0.09	Gueguen et al., 2016
Peru margin	0	0.59	0.09	Gueguen et al., 2016
Peru margin	0	0.57	0.09	Gueguen et al., 2016
Peru margin	0	0.55	0.09	Gueguen et al., 2016
Peru margin	0	0.63	0.09	Gueguen et al., 2016
Peru margin	0	0.64	0.09	Gueguen et al., 2016
Peru margin	0	0.60	0.09	Gueguen et al., 2016
Peru margin	0	0.59	0.09	Gueguen et al., 2016
Peru margin	0	0.56	0.09	Gueguen et al., 2016
Peru margin	0	0.65	0.09	Gueguen et al., 2016
Peru margin	0	0.72	0.09	Gueguen et al., 2016
Peru margin	0	0.73	0.09	Gueguen et al., 2016
Peru margin	0	0.73	0.09	Gueguen et al., 2016
Peru margin	0	0.64	0.09	Gueguen et al., 2016
Peru margin	0	0.57	0.09	Gueguen et al., 2016
Peru margin	0	0.42	0.09	Gueguen et al., 2016
Peru margin	0	0.52	0.09	Gueguen et al., 2016
Peru margin	0	0.53	0.09	Gueguen et al., 2016
Peru margin	0	0.44	0.09	Gueguen et al., 2016
Peru margin	0	0.46	0.09	Gueguen et al., 2016
Peru margin	0	0.52	0.09	Gueguen et al., 2016
Peru margin	0	0.40	0.09	Gueguen et al., 2016
Peru margin	0	0.47	0.09	Gueguen et al., 2016
Peru margin	0	0.42	0.09	Gueguen et al., 2016
Peru margin	0	0.55	0.09	Gueguen et al., 2016
Peru margin	0	0.75	0.09	Gueguen et al., 2016
Peru margin	0	0.80	0.09	Gueguen et al., 2016
Peru margin	0	0.75	0.09	Gueguen et al., 2016
Peru margin	0	0.88	0.09	Gueguen et al., 2016
Peru margin	0	0.83	0.09	Gueguen et al., 2016
Peru margin	0	0.67	0.09	Gueguen et al., 2016
Peru margin	0	0.74	0.09	Gueguen et al., 2016
Peru margin	0	0.91	0.09	Gueguen et al., 2016
Peru margin	0	0.75	0.09	Gueguen et al., 2016
Peru margin	0	0.82	0.09	Gueguen et al., 2016
Peru margin	0	0.75	0.09	Gueguen et al., 2016
Peru margin	0	0.62	0.09	Gueguen et al., 2016
Peru margin	0	0.50	0.09	Gueguen et al., 2016
Peru margin	0	0.47	0.09	Gueguen et al., 2016
Peru margin	0	0.44	0.09	Gueguen et al., 2016
Arabian Sea	0	-0.016	0.048	Schoenberg et al. 2008
Arabian Sea	0	-0.053	0.048	Schoenberg et al. 2008
Arabian Sea	0	-0.007	0.048	Schoenberg et al. 2008
Arabian Sea	0	-0.045	0.048	Schoenberg et al. 2008
Arabian Sea	0	-0.078	0.048	Schoenberg et al. 2008
Arabian Sea	0	0.009	0.048	Schoenberg et al. 2008
Cariaco Basin	0.02	0.31	0.09	Gueguen et al., 2016
Cariaco Basin	0.02	0.25	0.09	Gueguen et al., 2016
Cariaco Basin	0.02	0.28	0.09	Gueguen et al., 2016
Cariaco Basin	0.02	0.17	0.09	Gueguen et al., 2016
Cariaco Basin	0.02	0.29	0.09	Gueguen et al., 2016

SI Table 2. All Cr isotope data plotted on Figure 2 (main text)

SHALE/SILICICLASTIC Formation	Age (Ga)	(‰) $\delta^{53/52}Cr_{bulk}$	2se	Reference
Cariaco Basin	0.02	0.29	0.09	Gueguen et al., 2016
Cariaco Basin	0.02	0.17	0.09	Gueguen et al., 2016
Cariaco Basin	0.02	0.33	0.09	Reinhard et al., 2014
Cariaco Basin	0.02	0.35	0.09	Reinhard et al., 2014
Cariaco Basin	0.02	0.32	0.09	Reinhard et al., 2014
Cariaco Basin	0.02	0.34	0.09	Reinhard et al., 2014
Cariaco Basin	0.02	0.38	0.09	Reinhard et al., 2014
Cariaco Basin	0.02	0.27	0.09	Reinhard et al., 2014
Cariaco Basin	0.02	0.24	0.09	Reinhard et al., 2014
Cariaco Basin	0.02	0.38	0.09	Reinhard et al., 2014
Cariaco Basin	0.02	0.32	0.09	Reinhard et al., 2014
Cariaco Basin	0.02	0.37	0.09	Reinhard et al., 2014
Cariaco Basin	0.02	0.28	0.09	Reinhard et al., 2014
Cariaco Basin	0.02	0.34	0.09	Reinhard et al., 2014
Cariaco Basin	0.02	0.26	0.09	Reinhard et al., 2014
Cariaco Basin	0.02	0.17	0.09	Reinhard et al., 2014
Cariaco Basin	0.02	0.12	0.09	Reinhard et al., 2014
Cariaco Basin	0.02	0.09	0.09	Reinhard et al., 2014
OAE 2	0.094	1.20	0.09	Planavsky et al., 2014
OAE 2	0.094	0.72	0.09	Planavsky et al., 2014
OAE 2	0.094	0.70	0.09	Planavsky et al., 2014
OAE 2	0.094	0.82	0.09	Planavsky et al., 2014
OAE 2	0.094	0.62	0.09	Planavsky et al., 2014
OAE 2	0.094	0.99	0.09	Planavsky et al., 2014
OAE 2	0.094	0.89	0.09	Planavsky et al., 2014
OAE 2	0.094	0.37	0.09	Planavsky et al., 2014
OAE 2	0.094	0.66	0.09	Planavsky et al., 2014
OAE 2	0.094	0.58	0.09	Planavsky et al., 2014
OAE 2	0.094	0.65	0.09	Planavsky et al., 2014
OAE 2	0.094	0.27	0.09	Planavsky et al., 2014
OAE 2	0.094	0.32	0.09	Planavsky et al., 2014
OAE 2	0.094	0.24	0.09	Planavsky et al., 2014
OAE 2	0.094	0.25	0.09	Planavsky et al., 2014
OAE 2	0.094	1.11	0.09	Planavsky et al., 2014
OAE 2	0.094	1.23	0.09	Planavsky et al., 2014
OAE 2	0.094	0.86	0.09	Planavsky et al., 2014
OAE 2	0.094	1.05	0.09	Planavsky et al., 2014
OAE 2	0.094	1.06	0.09	Planavsky et al., 2014
OAE 2	0.094	1.26	0.09	Planavsky et al., 2014
OAE 2	0.094	1.27	0.09	Planavsky et al., 2014
OAE 2	0.094	1.22	0.09	Planavsky et al., 2014
OAE 2	0.094	1.26	0.09	Planavsky et al., 2014
OAE 2	0.094	1.20	0.09	Planavsky et al., 2014
OAE 2	0.094	1.14	0.09	Planavsky et al., 2014
OAE 2	0.094	1.08	0.09	Planavsky et al., 2014
OAE 2	0.094	1.14	0.09	Planavsky et al., 2014
OAE 2	0.094	1.03	0.09	Planavsky et al., 2014
OAE 2	0.094	1.13	0.09	Planavsky et al., 2014
Doldgeville Fm.	0.45	0.28	0.07	This study
Doldgeville Fm.	0.45	0.34	0.07	This study
Doldgeville Fm.	0.45	0.58	0.07	This study

SI Table 2. All Cr isotope data plotted on Figure 2 (main text)

SHALE/SILICICLASTIC Formation	Age (Ga)	(‰) $\delta^{53/52}Cr_{bulk}$	2se	Reference
Doldgeville Fm.	0.45	0.49	0.07	This study
Tal Group	0.55	0.23	0.07	This study
Tal Group	0.55	0.46	0.07	This study
Tal Group	0.55	0.55	0.07	This study
Tal Group	0.55	0.59	0.07	This study
Tal Group	0.55	0.16	0.07	This study
Tal Group	0.55	0.53	0.07	This study
Tal Group	0.55	0.17	0.07	This study
Yerbal Fm.	0.55	-0.04	0.09	Frei et al., 2013
Yerbal Fm.	0.55	-0.15	0.09	Frei et al., 2013
Yerbal Fm.	0.55	-0.21	0.08	Frei et al., 2013
Polanco Fm.	0.57	-0.11	0.02	Frei et al., 2013
Polanco Fm.	0.57	-0.21	0.01	Frei et al., 2013
Polanco Fm.	0.57	-0.17	0.03	Frei et al., 2013
Yerbal Fm.	0.57	-0.24	0.07	Frei et al., 2013
Yerbal Fm.	0.57	-0.22	0.02	Frei et al., 2013
Yerbal Fm.	0.57	-0.16		Frei et al., 2013
Yerbal Fm.	0.57	-0.2		Frei et al., 2013
Yerbal Fm.	0.57	-0.11		Frei et al., 2013
Yerbal Fm.	0.57	-0.1		Frei et al., 2013
Yerbal Fm.	0.57	-0.24		Frei et al., 2013
Yerbal Fm.	0.57	-0.14		Frei et al., 2013
Yerbal Fm.	0.57	-0.23		Frei et al., 2013
Yerbal Fm.	0.57	-0.25		Frei et al., 2013
Yerbal Fm.	0.57	-0.24		Frei et al., 2013
Yerbal Fm.	0.57	-0.24		Frei et al., 2013
Yerbal Fm.	0.57	-0.09		Frei et al., 2013
Yerbal Fm.	0.57	-0.06		Frei et al., 2013
Yerbal Fm.	0.57	-0.06		Frei et al., 2013
Yerbal Fm.	0.57	0.09		Frei et al., 2013
Yerbal Fm.	0.57	-0.12		Frei et al., 2013
Yerbal Fm.	0.57	-0.22		Frei et al., 2013
Yerbal Fm.	0.57	-0.06		Frei et al., 2013
Yerbal Fm.	0.57	-0.19		Frei et al., 2013
Yerbal Fm.	0.57	-0.23		Frei et al., 2013
Yerbal Fm.	0.57	-0.17		Frei et al., 2013
Yerbal Fm.	0.57	-0.27		Frei et al., 2013
Yerbal Fm.	0.57	-0.13		Frei et al., 2013
Yerbal Fm.	0.57	0.1		Frei et al., 2013
Yerbal Fm.	0.57	0.12		Frei et al., 2013
Yerbal Fm.	0.57	-0.13		Frei et al., 2013
Yerbal Fm.	0.57	0.09		Frei et al., 2013
Yerbal Fm.	0.57	-0.06		Frei et al., 2013
Yerbal Fm.	0.57	-0.13		Frei et al., 2013
Yerbal Fm.	0.57	-0.07		Frei et al., 2013
Yerbal Fm.	0.57	-0.09		Frei et al., 2013
Yerbal Fm.	0.57	-0.14		Frei et al., 2013
Yerbal Fm.	0.57	-0.1		Frei et al., 2013
Yerbal Fm.	0.57	-0.1		Frei et al., 2013
Yerbal Fm.	0.57	-0.11		Frei et al., 2013
Yerbal Fm.	0.57	-0.17		Frei et al., 2013

SI Table 2. All Cr isotope data plotted on Figure 2 (main text)

SHALE/SILICICLASTIC				
Formation	**Age (Ga)**	**(‰) $\delta^{53/52}Cr_{bulk}$**	**2se**	**Reference**
Polanco Fm.	0.57	0.29	0.05	Frei et al., 2013
Polanco Fm.	0.57	0.25	0.05	Frei et al., 2013
Polanco Fm.	0.57	0.22	0.03	Frei et al., 2013
Polanco Fm.	0.57	0.19	0.06	Frei et al., 2013
Polanco Fm.	0.57	0.06	0.05	Frei et al., 2013
Polanco Fm.	0.57	0.14	0.05	Frei et al., 2013
Polanco Fm.	0.57	-0.07	0.06	Frei et al., 2013
Polanco Fm.	0.57	-0.13	0.06	Frei et al., 2013
Polanco Fm.	0.57	-0.12	0.04	Frei et al., 2013
Polanco Fm.	0.57	-0.13	0.06	Frei et al., 2013
Polanco Fm.	0.57	-0.15	0.06	Frei et al., 2013
Polanco Fm.	0.57	-0.07	0.03	Frei et al., 2013
Polanco Fm.	0.57	-0.17	0.08	Frei et al., 2013
Polanco Fm.	0.57	-0.08	0.03	Frei et al., 2013
Polanco Fm.	0.57	-0.06	0.02	Frei et al., 2013
Polanco Fm.	0.57	0.1	0.03	Frei et al., 2013
Polanco Fm.	0.57	0.14	0.01	Frei et al., 2013
Polanco Fm.	0.57	0.11	0.05	Frei et al., 2013
Polanco Fm.	0.57	0.1	0.06	Frei et al., 2013
Polanco Fm.	0.57	0.19	0.06	Frei et al., 2013
Doushantou	0.63	-0.13	0.07	This study
Doushantou	0.63	-0.11	0.07	This study
Doushantou	0.63	-0.16	0.07	This study
Doushantou	0.63	-0.04	0.07	This study
Doushantou	0.63	-0.05	0.07	This study
Doushantou	0.63	-0.10	0.07	This study
Black River Dolomite	0.64	-0.16	0.07	This study
Black River Dolomite	0.64	0.10	0.07	This study
Black River Dolomite	0.7	0.14	0.07	This study
Black River Dolomite	0.7	0.16	0.07	This study
Black River Dolomite	0.7	0.12	0.07	This study
Black River Dolomite	0.8	0.09	0.07	This study
Black River Dolomite	0.8	0.23	0.07	This study
Black River Dolomite	0.8	0.24	0.07	This study
Chuar	0.74	0.70	0.07	This study
Chuar	0.74	0.73	0.07	This study
Chuar	0.74	0.68	0.07	This study
Chuar	0.74	0.70	0.07	This study
Chuar	0.74	0.58	0.07	This study
Chuar	0.74	0.62	0.07	This study
Chuar	0.74	0.73	0.07	This study
Chuar	0.74	0.60	0.07	This study
Chuar	0.74	0.52	0.07	This study
Chuar	0.74	0.15	0.07	This study
Shaler	0.7615	1.03	0.09	Planavsky et al., 2014
Shaler	0.7615	1.12	0.09	Planavsky et al., 2014
Shaler	0.7615	1.44	0.09	Planavsky et al., 2014
Shaler	0.7615	0.66	0.09	Planavsky et al., 2014
Shaler	0.7615	1.53	0.09	Planavsky et al., 2014
Shaler	0.7615	-0.07	0.09	Planavsky et al., 2014
Shaler	0.7615	-0.05	0.09	Planavsky et al., 2014

SI Table 2. All Cr isotope data plotted on Figure 2 (main text)

SHALE/SILICICLASTIC Formation	Age (Ga)	(‰) $\delta^{53/52}Cr_{bulk}$	2se	Reference
Shaler	0.7615	1.97	0.09	Planavsky et al., 2014
Shaler	0.7615	1.8	0.09	Planavsky et al., 2014
Shaler	0.7615	1.11	0.09	Planavsky et al., 2014
Shaler	0.7615	1.79	0.09	Planavsky et al., 2014
Shaler	0.7615	1.2	0.09	Planavsky et al., 2014
Shaler	0.7615	0.3	0.09	Planavsky et al., 2014
Shaler	0.7615	0.64	0.09	Planavsky et al., 2014
Shaler	0.7615	1.52	0.09	Planavsky et al., 2014
Shaler	0.7615	1.31	0.09	Planavsky et al., 2014
Shaler	0.7615	1.29	0.09	Planavsky et al., 2014
Shaler	0.7615	0.81	0.09	Planavsky et al., 2014
Shaler	0.7615	0.7	0.09	Planavsky et al., 2014
Shaler	0.7615	1.6	0.09	Planavsky et al., 2014
Shaler	0.7615	0.07	0.07	Planavsky et al., 2014
Shaler	0.7615	-0.14	0.07	Planavsky et al., 2014
Simla	0.83	-0.09	0.07	This study
Simla	0.83	-0.08	0.07	This study
Simla	0.83	-0.04	0.07	This study
Simla	0.83	0.04	0.07	This study
Simla	0.83	0.08	0.07	This study
Simla	0.83	0.10	0.07	This study
Simla	0.83	0.16	0.07	This study
Simla	0.83	0.09	0.07	This study
Arctic Bay	1.1	-0.07	0.07	This study
Arctic Bay	1.1	-0.12	0.07	This study
Arctic Bay	1.1	-0.14	0.07	This study
Arctic Bay	1.1	0.08	0.07	This study
Arctic Bay	1.1	0.01	0.07	This study
Arctic Bay	1.1	0.06	0.07	This study
Arctic Bay	1.1	0.07	0.07	This study
Arctic Bay	1.1	0.01	0.07	This study
Arctic Bay	1.1	-0.07	0.07	This study
Arctic Bay	1.1	-0.10	0.07	This study
Arctic Bay	1.1	-0.10	0.07	This study
Arctic Bay	1.1	-0.13	0.07	This study
Arctic Bay	1.1	-0.13	0.07	This study
Arctic Bay	1.1	-0.12	0.07	This study
Arctic Bay	1.1	-0.05	0.07	This study
Arctic Bay	1.1	-0.09	0.07	This study
Arctic Bay	1.1	-0.04	0.07	This study
Arctic Bay	1.1	-0.03	0.07	This study
Arctic Bay	1.1	0.09	0.07	This study
Arctic Bay	1.1	-0.11	0.07	This study
Arctic Bay	1.1	-0.03	0.07	This study
Arctic Bay	1.1	-0.09	0.07	This study
Arctic Bay	1.1	-0.10	0.07	This study
Arctic Bay	1.1	-0.13	0.07	This study
Arctic Bay	1.1	0.03	0.07	This study
Arctic Bay	1.1	-0.09	0.07	This study
Arctic Bay	1.1	-0.16	0.07	This study
Xiamaling	1.38	-0.05	0.07	This study

SI Table 2. All Cr isotope data plotted on Figure 2 (main text)

SHALE/SILICICLASTIC				
Formation	**Age (Ga)**	**(‰) $\delta^{53/52}Cr_{bulk}$**	**2se**	**Reference**
Xiamaling	1.38	-0.03	0.07	This study
Xiamaling	1.38	-0.09	0.07	This study
Xiamaling	1.38	-0.04	0.07	This study
Xiamaling	1.38	0.17	0.07	This study
Xiamaling	1.38	-0.19	0.07	This study
Velkerri	1.4	-0.14	0.07	This study
Velkerri	1.4	-0.01	0.07	This study
Velkerri	1.4	0.05	0.07	This study
Velkerri	1.4	-0.13	0.07	This study
Velkerri	1.4	-0.09	0.07	This study
Velkerri	1.4	-0.14	0.07	This study
Velkerri	1.4	-0.14	0.07	This study
Velkerri	1.4	-0.13	0.07	This study
Barney Creek	1.65	-0.17	0.07	This study
Barney Creek	1.65	-0.34	0.07	This study
Barney Creek	1.65	-0.11	0.07	This study
Barney Creek	1.65	-0.14	0.07	This study
Barney Creek	1.65	-0.13	0.07	This study
Barney Creek	1.65	-0.09	0.07	This study
Barney Creek	1.65	-0.14	0.07	This study
Barney Creek	1.65	-0.14	0.07	This study
Barney Creek	1.65	-0.11	0.07	This study
Barney Creek	1.65	-0.14	0.07	This study
Mt. Les Siltstone	1.65	-0.10	0.07	This study
Mt. Les Siltstone	1.65	-0.17	0.07	This study
Mt. Les Siltstone	1.65	-0.28	0.07	This study
Mt. Les Siltstone	1.65	-0.08	0.07	This study
Lady Lorreta	1.65	-0.18	0.07	This study
Lady Lorreta	1.65	-0.19	0.07	This study
Lady Lorreta	1.65	-0.18	0.07	This study
Lady Lorreta	1.65	-0.20	0.07	This study
Lady Lorreta	1.65	-0.17	0.07	This study
Lady Lorreta	1.65	-0.23	0.07	This study
Lady Lorreta	1.65	-0.20	0.07	This study
Damtha	1.7	-0.15	0.07	This study
Damtha	1.7	-0.06	0.07	This study
Damtha	1.7	-0.09	0.07	This study
Damtha	1.7	-0.14	0.07	This study
Damtha	1.7	-0.13	0.07	This study
Timeball Hill	2.32	-0.10	0.07	This study
Timeball Hill	2.32	-0.27	0.07	This study
Timeball Hill	2.32	-0.16	0.07	This study
Timeball Hill	2.32	-0.03	0.07	This study
Timeball Hill	2.32	-0.17	0.07	This study
Timeball Hill	2.32	-0.12	0.07	This study
Timeball Hill	2.32	-0.15	0.07	This study
Timeball Hill	2.32	-0.09	0.07	This study
Timeball Hill	2.32	-0.10	0.07	This study
Mt. McRae Shale	2.5	-0.15	0.07	This study
Mt. McRae Shale	2.5	-0.08	0.07	This study
Mt. McRae Shale	2.5	-0.19	0.07	This study

SI Table 2. All Cr isotope data plotted on Figure 2 (main text)

SHALE/SILICICLASTIC Formation	Age (Ga)	(‰) $\delta^{53/52}Cr_{bulk}$	2se	Reference
Mt. McRae Shale	2.5	-0.10	0.07	This study
Mt. McRae Shale	2.5	-0.17	0.07	This study
Mt. McRae Shale	2.5	0.01	0.07	This study
Mt. McRae Shale	2.5	-0.12	0.07	This study
Mt. McRae Shale	2.5	-0.23	0.07	This study
Mt. McRae Shale	2.5	-0.10	0.07	This study
Mt. McRae Shale	2.5	-0.08	0.07	This study
Mt. McRae Shale	2.5	-0.11	0.07	This study
Mt. McRae Shale	2.5	-0.15	0.07	This study
Mt. McRae Shale	2.5	-0.19	0.07	This study
Mt. McRae Shale	2.5	-0.09	0.07	This study
Mt. McRae Shale	2.5	-0.02	0.07	This study
Mt. McRae Shale	2.5	-0.01	0.07	This study
Mt. McRae Shale	2.5	-0.10	0.07	This study
Mt. McRae Shale	2.5	-0.13	0.07	This study
Mt. McRae Shale	2.5	-0.10	0.07	This study
Mt. Sylvia	2.55	-0.09	0.07	This study
Mt. Sylvia	2.55	-0.08	0.07	This study
Mt. Sylvia	2.55	-0.09	0.07	This study
Mt. Sylvia	2.55	-0.08	0.07	This study
Roy Hill Shale mbr.	2.7	-0.12	0.07	This study
Roy Hill Shale mbr.	2.7	-0.16	0.07	This study
Roy Hill Shale mbr.	2.7	-0.13	0.07	This study
Roy Hill Shale mbr.	2.7	-0.14	0.07	This study
Roy Hill Shale mbr.	2.7	-0.11	0.07	This study
Roy Hill Shale mbr.	2.7	-0.17	0.07	This study
Roy Hill Shale mbr.	2.7	-0.09	0.07	This study
Roy Hill Shale mbr.	2.7	-0.08	0.07	This study
Roy Hill Shale mbr.	2.7	-0.10	0.07	This study
Roy Hill Shale mbr.	2.7	-0.13	0.07	This study
Roy Hill Shale mbr.	2.7	-0.14	0.07	This study
Roy Hill Shale mbr.	2.7	-0.07	0.07	This study
Roy Hill Shale mbr.	2.7	-0.15	0.07	This study
Roy Hill Shale mbr.	2.7	-0.02	0.07	This study
Roy Hill Shale mbr.	2.7	-0.11	0.07	This study
Roy Hill Shale mbr.	2.7	-0.14	0.07	This study
Roy Hill Shale mbr.	2.7	-0.14	0.07	This study
Roy Hill Shale mbr.	2.7	-0.11	0.07	This study
Roy Hill Shale mbr.	2.7	-0.11	0.07	This study
Roy Hill Shale mbr.	2.7	-0.13	0.07	This study
Roy Hill Shale mbr.	2.7	-0.14	0.07	This study
Roy Hill Shale mbr.	2.7	-0.16	0.07	This study
Roy Hill Shale mbr.	2.7	-0.13	0.07	This study
Roy Hill Shale mbr.	2.7	-0.13	0.07	This study
Roy Hill Shale mbr.	2.7	-0.12	0.07	This study
Roy Hill Shale mbr.	2.7	-0.15	0.07	This study
Roy Hill Shale mbr.	2.7	-0.12	0.07	This study
Roy Hill Shale mbr.	2.7	-0.07	0.07	This study
Roy Hill Shale mbr.	2.7	-0.11	0.07	This study
Roy Hill Shale mbr.	2.7	-0.09	0.07	This study
Roy Hill Shale mbr.	2.7	-0.11	0.07	This study

SI Table 2. All Cr isotope data plotted on Figure 2 (main text)

SHALE/SILICICLASTIC Formation	Age (Ga)	(‰) $\delta^{53/52}Cr_{bulk}$	2se	Reference
Roy Hill Shale mbr.	2.7	-0.11	0.07	This study
Roy Hill Shale mbr.	2.7	-0.13	0.07	This study
Roy Hill Shale mbr.	2.7	-0.11	0.07	This study
Roy Hill Shale mbr.	2.7	-0.13	0.07	This study
Roy Hill Shale mbr.	2.7	-0.10	0.07	This study
Roy Hill Shale mbr.	2.7	0.03	0.07	This study
Roy Hill Shale mbr.	2.7	-0.10	0.07	This study
Roy Hill Shale mbr.	2.7	0.05	0.07	This study
Roy Hill Shale mbr.	2.7	-0.02	0.07	This study
Roy Hill Shale mbr.	2.7	-0.12	0.07	This study
Roy Hill Shale mbr.	2.7	-0.15	0.07	This study
Roy Hill Shale mbr.	2.7	-0.16	0.07	This study
Roy Hill Shale mbr.	2.7	-0.21	0.07	This study
Roy Hill Shale mbr.	2.7	-0.19	0.07	This study
Roy Hill Shale mbr.	2.7	-0.23	0.07	This study
Roy Hill Shale mbr.	2.7	-0.26	0.07	This study
Hardey Fm.	2.76	-0.11	0.062	Wille et al., 2013
Hardey Fm.	2.76	-0.12	0.107	Wille et al., 2013
Hardey Fm.	2.76	-0.15	0.02	Wille et al., 2013
Hardey Fm.	2.76	-0.11	0.065	Wille et al., 2013
Mt. Roe Basalt	2.77	-0.05	0.073	Wille et al., 2013
Mt. Roe Basalt	2.77	-0.05	0.098	Wille et al., 2013
Mt. Roe Basalt	2.77	-0.14	0.061	Wille et al., 2013
Mt. Roe Basalt	2.77	-0.16	0.118	Wille et al., 2013
Nullagine Gp.	2.94	0.03	0.16	Wille et al., 2013
Nullagine Gp.	2.94	-0.16	0.057	Wille et al., 2013
Nullagine Gp.	2.94	-0.03	0.094	Wille et al., 2013
Nullagine Gp.	2.94	-0.16	0.069	Wille et al., 2013
Nullagine Gp.	2.94	-0.09	0.041	Wille et al., 2013
Duffer Fm.	3.46	-0.07	0.038	Wille et al., 2013
Duffer Fm.	3.46	-0.14	0.054	Wille et al., 2013
Duffer Fm.	3.46	-0.10	0.071	Wille et al., 2013
Duffer Fm.	3.46	-0.13	0.047	Wille et al., 2013
Duffer Fm.	3.46	-0.06	0.084	Wille et al., 2013
Duffer Fm.	3.46	-0.07	0.04	Wille et al., 2013
Duffer Fm.	3.46	-0.14	0.05	Wille et al., 2013
Duffer Fm.	3.46	-0.10	0.07	Wille et al., 2013
Duffer Fm.	3.46	-0.13	0.05	Wille et al., 2013
Duffer Fm.	3.46	-0.06	0.08	Wille et al., 2013

SI Table 2. All Cr isotope data plotted on Figure 2 (main text)

IRON FORMATIONS/IRONSTONES				
Formation	**Age (Ga)**	**(‰) $\delta^{53/52}Cr_{bulk}$**	**2se**	**Reference**
Langrial	0.062	0.5	0.09	Planavsky et al., 2014
Langrial	0.062	0.56	0.09	Planavsky et al., 2014
Langrial	0.062	0.48	0.09	Planavsky et al., 2014
Langrial	0.062	0.25	0.09	Planavsky et al., 2014
Langrial	0.062	0.38	0.09	Planavsky et al., 2014
Langrial	0.062	0.6	0.09	Planavsky et al., 2014
Langrial	0.062	0.55	0.09	Planavsky et al., 2014
Rashby Ironstone	0.18	0.57	0.09	Planavsky et al., 2014
Cleveland Ironston	0.18	0.11	0.09	Planavsky et al., 2014
Cleveland Ironston	0.18	-0.01	0.09	Planavsky et al., 2014
Scunthorpe	0.19	0.62	0.09	Planavsky et al., 2014
Scunthorpe	0.19	0.48	0.09	Planavsky et al., 2014
Scunthorpe	0.19	0.37	0.09	Planavsky et al., 2014
Scunthorpe	0.19	0.05	0.09	Planavsky et al., 2014
Cap de la Chèvre	0.46	-0.08	0.09	Planavsky et al., 2014
Cap de la Chèvre	0.46	-0.03	0.09	Planavsky et al., 2014
Cap de la Chèvre	0.46	-0.09	0.09	Planavsky et al., 2014
Cap de la Chèvre	0.46	0.11	0.09	Planavsky et al., 2014
Cap de la Chèvre	0.46	-0.03	0.09	Planavsky et al., 2014
Red Mountain	0.44	0.15	0.09	Planavsky et al., 2014
Red Mountain	0.44	0.48	0.09	Planavsky et al., 2014
Red Mountain	0.44	0.08	0.09	Planavsky et al., 2014
Red Mountain	0.44	0.39	0.09	Planavsky et al., 2014
Red Mountain	0.44	0.65	0.09	Planavsky et al., 2014
Aok	1.015	-0.08	0.09	Planavsky et al., 2014
Aok	1.015	-0.1	0.09	Planavsky et al., 2014
Sherwin	1.4625	-0.13	0.09	Planavsky et al., 2014
Sherwin	1.4625	-0.19	0.09	Planavsky et al., 2014
Sherwin	1.4625	-0.07	0.09	Planavsky et al., 2014
Sherwin	1.4625	-0.01	0.09	Planavsky et al., 2014
Sherwin	1.4625	-0.05	0.09	Planavsky et al., 2014
Sherwin	1.4625	-0.02	0.09	Planavsky et al., 2014
Sherwin	1.4625	-0.07	0.09	Planavsky et al., 2014
Sherwin	1.4625	-0.05	0.09	Planavsky et al., 2014
Sherwin	1.4625	-0.1	0.09	Planavsky et al., 2014
Sherwin	1.4625	-0.15	0.09	Planavsky et al., 2014
Sherwin	1.4625	-0.13	0.09	Planavsky et al., 2014
Sherwin	1.4625	-0.02	0.09	Planavsky et al., 2014
Sherwin	1.4625	-0.01	0.09	Planavsky et al., 2014
Sherwin	1.4625	-0.03	0.09	Planavsky et al., 2014
Sherwin	1.4625	-0.03	0.09	Planavsky et al., 2014
Freedom	1.67	-0.11	0.09	Planavsky et al., 2014
Freedom	1.67	-0.12	0.09	Planavsky et al., 2014
Freedom	1.67	-0.18	0.09	Planavsky et al., 2014
Freedom	1.67	-0.03	0.09	Planavsky et al., 2014
Freedom	1.67	-0.1	0.09	Planavsky et al., 2014
Freedom	1.67	-0.09	0.09	Planavsky et al., 2014
Chuanlinggou	1.699	-0.16	0.09	Planavsky et al., 2014
Chuanlinggou	1.699	-0.17	0.09	Planavsky et al., 2014
Chuanlinggou	1.699	-0.1	0.09	Planavsky et al., 2014
Chuanlinggou	1.699	-0.2	0.09	Planavsky et al., 2014

SI Table 2. All Cr isotope data plotted on Figure 2 (main text)

IRON FORMATIONS/IRONSTONES				
Formation	**Age (Ga)**	**(‰) $\delta^{53/52}Cr_{bulk}$**	**2se**	**Reference**
Chuanlinggou	1.699	-0.05	0.09	Planavsky et al., 2014
Chuanlinggou	1.699	-0.13	0.09	Planavsky et al., 2014
Chuanlinggou	1.699	-0.16	0.09	Planavsky et al., 2014
Chuanlinggou	1.699	-0.18	0.09	Planavsky et al., 2014
Chuanlinggou	1.699	-0.21	0.09	Planavsky et al., 2014
Chuanlinggou	1.699	0.03	0.09	Planavsky et al., 2014
Timeball Hill	2.327	-0.07	0.09	Planavsky et al., 2014
Timeball Hill	2.327	-0.09	0.09	Planavsky et al., 2014
Timeball Hill	2.327	-0.05	0.09	Planavsky et al., 2014
Timeball Hill	2.327	-0.08	0.09	Planavsky et al., 2014
Timeball Hill	2.327	-0.03	0.09	Planavsky et al., 2014
Timeball Hill	2.327	-0.06	0.09	Planavsky et al., 2014
Timeball Hill	2.327	-0.08	0.09	Planavsky et al., 2014
Timeball Hill	2.327	-0.1	0.09	Planavsky et al., 2014
Timeball Hill	2.327	-0.15	0.09	Planavsky et al., 2014
Timeball Hill	2.327	-0.05	0.09	Planavsky et al., 2014
Timeball Hill	2.327	-0.13	0.09	Planavsky et al., 2014
Timeball Hill	2.327	-0.1	0.09	Planavsky et al., 2014
Sinqeni	2.975	-0.09	0.09	Planavsky et al., 2014
Sinqeni	2.975	-0.11	0.09	Planavsky et al., 2014
Sinqeni	2.975	-0.11	0.09	Planavsky et al., 2014
Sinqeni	2.975	-0.15	0.09	Planavsky et al., 2014
Sinqeni	2.975	-0.08	0.09	Planavsky et al., 2014
Sinqeni	2.975	0.09	0.09	Planavsky et al., 2014
Mozaan Gp	2.9	-0.12	0.09	Planavsky et al., 2014
Mozaan Gp	2.9	-0.11	0.09	Planavsky et al., 2014
Mozaan Gp	2.9	-0.07	0.09	Planavsky et al., 2014
Mozaan Gp	2.9	-0.05	0.09	Planavsky et al., 2014
Mozaan Gp	2.9	-0.08	0.09	Planavsky et al., 2014
Mozaan Gp	2.9	-0.09	0.09	Planavsky et al., 2014
Mozaan Gp	2.9	-0.05	0.09	Planavsky et al., 2014
Mozaan Gp	2.9	-0.15	0.09	Planavsky et al., 2014
Mozaan Gp	2.9	-0.10	0.09	Planavsky et al., 2014
Mozaan Gp	2.9	-0.08	0.09	Planavsky et al., 2014
Mozaan Gp	2.9	-0.07	0.09	Planavsky et al., 2014
Cerro Espuelitas Fm.	0.55	1.34	0.14	Frei et al., 2009
Cerro Espuelitas Fm.	0.55	1.32	0.04	Frei et al., 2009
Cerro Espuelitas Fm.	0.55	0.52	0.13	Frei et al., 2009
Cerro Espuelitas Fm.	0.55	0.44	0.11	Frei et al., 2009
Yerbal Fm.	0.57	3.22	0.03	Frei et al., 2009
Yerbal Fm.	0.57	3.39	0.04	Frei et al., 2009
Yerbal Fm.	0.57	3.25	0.03	Frei et al., 2009
Yerbal Fm.	0.57	4.92	0.02	Frei et al., 2009
Yerbal Fm.	0.57	5	0.02	Frei et al., 2009
Yerbal Fm.	0.57	4.51	0.03	Frei et al., 2009
Yerbal Fm.	0.57	3.12	0.18	Frei et al., 2009
Yerbal Fm.	0.57	2.09	0.07	Frei et al., 2009
Yerbal Fm.	0.57	2.16	0.08	Frei et al., 2009
Yerbal Fm.	0.57	1.9	0.1	Frei et al., 2009
Yerbal Fm.	0.57	2.16	0.06	Frei et al., 2009
Yerbal Fm.	0.57	1.89	0.09	Frei et al., 2009

SI Table 2. All Cr isotope data plotted on Figure 2 (main text)

IRON FORMATIONS/IRONSTONES				
Formation	**Age (Ga)**	**(‰) $\delta^{53/52}Cr_{bulk}$**	**2se**	**Reference**
Yerbal Fm.	0.57	2.03	0.04	Frei et al., 2009
Yerbal Fm.	0.57	0.31	0.03	Frei et al., 2009
Yerbal Fm.	0.57	0.98	0.05	Frei et al., 2009
Yerbal Fm.	0.57	1.1	0.05	Frei et al., 2009
Yerbal Fm.	0.57	1.1	0.02	Frei et al., 2009
Yerbal Fm.	0.57	0.96	0.02	Frei et al., 2009
Yerbal Fm.	0.57	0.85	0.07	Frei et al., 2009
Yerbal Fm.	0.57	0.29	0.03	Frei et al., 2009
Yerbal Fm.	0.57	0.32	0.04	Frei et al., 2009
Yerbal Fm.	0.57	0.27	0.02	Frei et al., 2009
Yerbal Fm.	0.57	0.65	0.03	Frei et al., 2009
Yerbal Fm.	0.57	0.62	0.04	Frei et al., 2009
Yerbal Fm.	0.57	1.06	0.03	Frei et al., 2009
Yerbal Fm.	0.57	1.19	0.03	Frei et al., 2009
Yerbal Fm.	0.57	1.21	0.17	Frei et al., 2009
Cerro Espuelitas Fm.	0.55	1.34	0.14	Frei et al., 2009
Cerro Espuelitas Fm.	0.55	1.32	0.04	Frei et al., 2009
Cerro Espuelitas Fm.	0.55	0.52	0.13	Frei et al., 2009
Cerro Espuelitas Fm.	0.55	0.44	0.11	Frei et al., 2009
Rapitan Fm.	0.74	0.9	0.03	Frei et al., 2009
Rapitan Fm.	0.74	0.96	0.04	Frei et al., 2009
Rapitan Fm.	0.74	0.9	0.05	Frei et al., 2009
Negaunee IF	1.874	-0.25	0.06	Frei et al., 2009
Negaunee IF	1.874	-0.14	0.05	Frei et al., 2009
Rochford Fm.	1.88	-0.25	0.02	Frei et al., 2009
Rochford Fm.	1.88	-0.17	0.03	Frei et al., 2009
Rochford Fm.	1.88	-0.17	0.04	Frei et al., 2009
Gunflint Fm.	1.84	0.21	0.02	Frei et al., 2009
Gunflint Fm.	1.84	0.08	0.04	Frei et al., 2009
Gunflint Fm.	1.84	0.04	0.05	Frei et al., 2009
Gunflint Fm.	1.84	0.14	0.02	Frei et al., 2009
Gunflint Fm.	1.84	0.04	0.08	Frei et al., 2009
Gunflint Fm.	1.84	0.06	0.02	Frei et al., 2009
Gunflint Fm.	1.84	0.08	0.02	Frei et al., 2009
Gunflint Fm.	1.878	-0.19	0.02	Frei et al., 2009
Gunflint Fm.	1.878	-0.18	0.02	Frei et al., 2009
Gunflint Fm.	1.878	-0.13	0.04	Frei et al., 2009
Gunflint Fm.	1.878	-0.11	0.03	Frei et al., 2009
Gunflint Fm.	1.878	-0.23	0.02	Frei et al., 2009
Gunflint Fm.	1.878	-0.15	0.04	Frei et al., 2009
Gunflint Fm.	1.878	-0.18	0.02	Frei et al., 2009
Gunflint Fm.	1.878	-0.11	0.02	Frei et al., 2009
Gunflint Fm.	1.878	-0.24	0.04	Frei et al., 2009
Gunflint Fm.	1.878	-0.26	0.02	Frei et al., 2009
Gunflint Fm.	1.878	-0.22	0.05	Frei et al., 2009
Gunflint Fm.	1.878	-0.12	0.08	Frei et al., 2009
Bailadilla Gp.	2.1	-0.11	0.04	Frei et al., 2009
Bailadilla Gp.	2.1	-0.08	0.02	Frei et al., 2009
Bailadilla Gp.	2.1	-0.12	0.27	Frei et al., 2009
Bailadilla Gp.	2.1	-0.12	0.04	Frei et al., 2009
Bailadilla Gp.	2.1	-0.13	0.04	Frei et al., 2009

SI Table 2. All Cr isotope data plotted on Figure 2 (main text)

IRON FORMATIONS/IRONSTONES				
Formation	**Age (Ga)**	**(‰) $\delta^{53/52}Cr_{bulk}$**	**2se**	**Reference**
Bailadilla Gp.	2.1	-0.06	0.03	Frei et al., 2009
Bailadilla Gp.	2.1	-0.13	0.02	Frei et al., 2009
Rochford Fm.	2.015	-0.06	0.04	Frei et al., 2009
Rochford Fm.	2.015	-0.01	0.04	Frei et al., 2009
Rochford Fm.	2.015	-0.06	0.03	Frei et al., 2009
Rochford Fm.	2.015	-0.09	0.02	Frei et al., 2009
Rochford Fm.	2.015	-0.13	0.05	Frei et al., 2009
Rochford Fm.	2.015	-0.08	0.08	Frei et al., 2009
Rochford Fm.	2.015	0.03	0.08	Frei et al., 2009
Rochford Fm.	2.015	0	0.02	Frei et al., 2009
Rochford Fm.	2.015	-0.12	0.07	Frei et al., 2009
Rochford Fm.	2.015	-0.09	0.02	Frei et al., 2009
Rochford Fm.	2.015	-0.11	0.02	Frei et al., 2009
Rochford Fm.	2.015	-0.09	0.04	Frei et al., 2009
Rochford Fm.	2.015	-0.09	0.03	Frei et al., 2009
Rochford Fm.	2.015	-0.07	0.06	Frei et al., 2009
Homestake Fm. Equivalent (unname	2.015	-0.17	0.05	Frei et al., 2009
Homestake Fm. Equivalent (unname	2.015	-0.14	0.04	Frei et al., 2009
Homestake Fm. Equivalent (unname	2.015	-0.17	0.04	Frei et al., 2009
Homestake Fm. Equivalent (unname	2.015	-0.14	0.04	Frei et al., 2009
Homestake Fm. Equivalent (unname	2.015	-0.1	0.05	Frei et al., 2009
Homestake Fm. Equivalent (unname	2.015	-0.05	0.05	Frei et al., 2009
Homestake Fm. Equivalent (unname	2.015	-0.14	0.05	Frei et al., 2009
Amalia-Kraaipan terrain	2.45	-0.07	0.05	Frei et al., 2009
Amalia-Kraaipan terrain	2.45	-0.11	0.01	Frei et al., 2009
Amalia-Kraaipan terrain	2.45	-0.16	0.04	Frei et al., 2009
Benchmark Fm.	2.48	-0.1	0.02	Frei et al., 2009
Benchmark Fm.	2.48	-0.21	0.02	Frei et al., 2009
Kuruman Fm.	2.47	0.01	0.03	Frei et al., 2009
Kuruman Fm.	2.47	-0.07	0.04	Frei et al., 2009
Kuruman Fm.	2.47	-0.1	0.04	Frei et al., 2009
Kuruman Fm.	2.47	-0.09	0.08	Frei et al., 2009
Kuruman Fm.	2.47	-0.18	0.08	Frei et al., 2009
Kuruman Fm.	2.47	-0.11	0.07	Frei et al., 2009
Kuruman Fm.	2.47	-0.15	0.03	Frei et al., 2009
Cherry Creek Suite	2.61	0.11	0.04	Frei et al., 2009
Cherry Creek Suite	2.61	0.28	0.29	Frei et al., 2009
Cherry Creek Suite	2.61	0.23	0.21	Frei et al., 2009
Tati Greenstone Belt	2.7	-0.2	0.03	Frei et al., 2009
Tati Greenstone Belt	2.7	-0.06	0.05	Frei et al., 2009
Tati Greenstone Belt	2.7	-0.09	0.05	Frei et al., 2009
Tati Greenstone Belt	2.7	-0.16	0.02	Frei et al., 2009
Boston IF	2.7	0.21	0.04	Frei et al., 2009
Terragami IF	2.7	-0.04	0.06	Frei et al., 2009
Terragami IF	2.7	0.05	0.06	Frei et al., 2009
Terragami IF	2.7	0.04	0.12	Frei et al., 2009
Cheshire Fm.	2.601	0.07	0.06	Frei et al., 2009
Cheshire Fm.	2.601	0.08	0.04	Frei et al., 2009
Itacaiunas Supergp., Carajas Fm.	2.74	-0.12	0.07	Frei et al., 2009
Itacaiunas Supergp., Carajas Fm.	2.74	-0.14	0.06	Frei et al., 2009
Minto Block, Superior Province	2.83	-0.19	0.03	Frei et al., 2009

SI Table 2. All Cr isotope data plotted on Figure 2 (main text)

IRON FORMATIONS/IRONSTONES				
Formation	**Age (Ga)**	**(‰) $\delta^{53/52}Cr_{bulk}$**	**2se**	**Reference**
Minto Block, Superior Province	2.83	-0.09	0.05	Frei et al., 2009
Nemo IF	2.9	-0.11	0.04	Frei et al., 2009
Tomka-Daitari Belt, Singhbhum Crat	3.51	-0.17	0.05	Frei et al., 2009
Isua Greenstone Belt	3.75	-0.2	0.05	Frei et al., 2009
Isua Greenstone Belt	3.75	-0.21	0.04	Frei et al., 2009
Isua Greenstone Belt	3.75	-0.17	0.02	Frei et al., 2009
Isua Greenstone Belt	3.75	-0.25	0.04	Frei et al., 2009
Isua Greenstone Belt	3.75	-0.15	0.03	Frei et al., 2009
Isua Greenstone Belt	3.75	-0.16	0.03	Frei et al., 2009
Isua Greenstone Belt	3.75	-0.17	0.06	Frei et al., 2009
Isua Greenstone Belt	3.75	-0.13	0.03	Frei et al., 2009
Isua Greenstone Belt	3.75	-0.25	0.03	Frei et al., 2009
Isua Greenstone Belt	3.75	-0.22	0.04	Frei et al., 2009
Mozaan BIF	2.9	0.18	0.12	Crowe et al., 2013
Mozaan BIF	2.9	-0.2	0.12	Crowe et al., 2013
Mozaan BIF	2.9	-0.21	0.12	Crowe et al., 2013
Mozaan BIF	2.9	0	0.12	Crowe et al., 2013
Mozaan BIF	2.9	-0.18	0.12	Crowe et al., 2013
Mozaan BIF	2.9	-0.23	0.12	Crowe et al., 2013
Mozaan BIF	2.9	0.26	0.14	Crowe et al., 2013
Mozaan BIF	2.9	0.17	0.12	Crowe et al., 2013
Mozaan BIF	2.9	0.16	0.13	Crowe et al., 2013
Mozaan BIF	2.9	-0.12	0.12	Crowe et al., 2013
Mozaan BIF	2.9	0.28	0.12	Crowe et al., 2013
Cerro Espeulitas Fm.	0.55	0.64	0.09	Frei et al., 2011
Cerro Espeulitas Fm.	0.55	0.62	0.11	Frei et al., 2011
Cerro Espeulitas Fm.	0.55	0.24	0.09	Frei et al., 2011
Yerbal Fm.	0.55	1.17	0.12	Frei et al., 2011
Yerbal Fm.	0.55	3.64	0.13	Frei et al., 2011
Yerbal Fm.	0.55	0.99	0.11	Frei et al., 2011
Yerbal Fm.	0.55	0.27	0.09	Frei et al., 2011
Yerbal Fm.	0.55	0.11	0.07	Frei et al., 2011
Yerbal Fm.	0.55	1.13	0.13	Frei et al., 2011
Yerbal Fm.	0.55	1.24	0.12	Frei et al., 2011
Yerbal Fm.	0.55	1.74	0.14	Frei et al., 2011
Yerbal Fm.	0.55	0.63	0.09	Frei et al., 2011
Yerbal Fm.	0.57	0.52		Frei et al., 2011
Yerbal Fm.	0.57	0.6		Frei et al., 2011
Yerbal Fm.	0.57	0.67		Frei et al., 2011
Yerbal Fm.	0.57	1.05		Frei et al., 2011
Yerbal Fm.	0.57	1.08		Frei et al., 2011
Yerbal Fm.	0.57	1.18		Frei et al., 2011
Gunflint	1.9	0.39	0.04	Frei et al., 2011
Gunflint	1.9	0.06	0.03	Frei et al., 2011
Isua Greenstone Belt	3.75	0.06	0.06	Frei et al., 2016
Isua Greenstone Belt	3.75	0.31	0.06	Frei et al., 2016
Isua Greenstone Belt	3.75	0.09	0.06	Frei et al., 2016
Isua Greenstone Belt	3.75	0.42	0.06	Frei et al., 2016
Isua Greenstone Belt	3.75	0.03	0.06	Frei et al., 2016
Isua Greenstone Belt	3.75	0.09	0.06	Frei et al., 2016
Isua Greenstone Belt	3.75	0.04	0.06	Frei et al., 2016

SI Table 2. All Cr isotope data plotted on Figure 2 (main text)

IRON FORMATIONS/IRONSTONES				
Formation	**Age (Ga)**	**(‰) $\delta^{53/52}Cr_{bulk}$**	**2se**	**Reference**
Isua Greenstone Belt	3.75	0.07	0.06	Frei et al., 2016
Isua Greenstone Belt	3.75	0.15	0.05	Frei et al., 2016
Isua Greenstone Belt	3.75	0.07	0.04	Frei et al., 2016
Isua Greenstone Belt	3.75	0.09	0.04	Frei et al., 2016
Isua Greenstone Belt	3.75	-0.04	0.06	Frei et al., 2016
Isua Greenstone Belt	3.75	-0.04	0.06	Frei et al., 2016
Isua Greenstone Belt	3.75	0.03	0.08	Frei et al., 2016
Isua Greenstone Belt	3.75	-0.05	0.07	Frei et al., 2016
Isua Greenstone Belt	3.75	0.07	0.07	Frei et al., 2016
Isua Greenstone Belt	3.75	-0.04	0.06	Frei et al., 2016
Isua Greenstone Belt	3.75	-0.09	0.07	Frei et al., 2016
Isua Greenstone Belt	3.75	0.01	0.07	Frei et al., 2016
Isua Greenstone Belt	3.75	0.17	0.05	Frei et al., 2016
Isua Greenstone Belt	3.75	0.17	0.06	Frei et al., 2016
Isua Greenstone Belt	3.75	0.04	0.06	Frei et al., 2016
Isua Greenstone Belt	3.75	0.15	0.06	Frei et al., 2016
Isua Greenstone Belt	3.75	0.13	0.06	Frei et al., 2016
Isua Greenstone Belt	3.75	0.04	0.08	Frei et al., 2016
Isua Greenstone Belt	3.75	0.16	0.07	Frei et al., 2016
Isua Greenstone Belt	3.75	0.15	0.08	Frei et al., 2016
Isua Greenstone Belt	3.75	0.05	0.07	Frei et al., 2016
Isua Greenstone Belt	3.75	0.19	0.08	Frei et al., 2016
Isua Greenstone Belt	3.75	-0.10	0.04	Frei et al., 2016
Isua Greenstone Belt	3.75	-0.03	0.06	Frei et al., 2016
Isua Greenstone Belt	3.75	0.03	0.06	Frei et al., 2016
Isua Greenstone Belt	3.75	0.06	0.04	Frei et al., 2016
Isua Greenstone Belt	3.75	-0.02	0.03	Frei et al., 2016
Isua Greenstone Belt	3.75	-0.08	0.07	Frei et al., 2016
Isua Greenstone Belt	3.75	-0.04	0.06	Frei et al., 2016
Isua Greenstone Belt	3.75	0.16	0.06	Frei et al., 2016
Isua Greenstone Belt	3.75	0.10	0.06	Frei et al., 2016
Isua Greenstone Belt	3.75	-0.04	0.06	Frei et al., 2016
Isua Greenstone Belt	3.75	0.09	0.06	Frei et al., 2016
Isua Greenstone Belt	3.75	-0.12	0.07	Frei et al., 2016
Isua Greenstone Belt	3.75	-0.09	0.07	Frei et al., 2016
Isua Greenstone Belt	3.75	0.07	0.06	Frei et al., 2016
Isua Greenstone Belt	3.75	0.07	0.06	Frei et al., 2016
Isua Greenstone Belt	3.75	-0.01	0.06	Frei et al., 2016
Isua Greenstone Belt	3.75	-0.04	0.08	Frei et al., 2016
Isua Greenstone Belt	3.75	0.08	0.06	Frei et al., 2016
Isua Greenstone Belt	3.75	-0.07	0.08	Frei et al., 2016
Isua Greenstone Belt	3.75	-0.12	0.06	Frei et al., 2016
Isua Greenstone Belt	3.75	-0.12	0.06	Frei et al., 2016
Isua Greenstone Belt	3.75	-0.32	0.06	Frei et al., 2016
Isua Greenstone Belt	3.75	-0.14	0.06	Frei et al., 2016
Isua Greenstone Belt	3.75	-0.54	0.06	Frei et al., 2016
Isua Greenstone Belt	3.75	0.08	0.07	Frei et al., 2016
Isua Greenstone Belt	3.75	-0.16	0.06	Frei et al., 2016
Isua Greenstone Belt	3.75	0.04	0.07	Frei et al., 2016
Isua Greenstone Belt	3.75	-0.43	0.06	Frei et al., 2016

SI Table 2. All Cr isotope data plotted on Figure 2 (main text)

IRON FORMATIONS/IRONSTONES				
Formation	**Age (Ga)**	**(‰) $\delta^{53/52}Cr_{bulk}$**	**2se**	**Reference**

SI Table 2. All Cr isotope data plotted on Figure 2 (main text)

IRON FORMATIONS/IRONSTONES				
Formation	**Age (Ga)**	**(‰) $\delta^{53/52}Cr_{bulk}$**	**2se**	**Reference**